

**DEVELOPING AEROSOL JET PRINTABLE REGENERATED SILK FIBROIN
SOLUTION**

A Thesis
Presented to
The Academic Faculty

by

Yuhan Xiao

In Partial Fulfillment
of the Requirements for the Degree
Master of Science in the
GEORGE W. WOODRUFF SCHOOL OF MECHANICAL ENGINEERING

Georgia Institute of Technology
MAY 2019

COPYRIGHT © 2019 BY YUHAN XIAO

**DEVELOPING A REGENERATED SILK FIBROIN SOLUTION TO BE
AEROSOL JET PRINTABLE**

Approved by:

Dr. Tequila A. L. Harris, Advisor
School of Mechanical Engineering
Georgia Institute of Technology

Dr. Kyriaki Kalaitzidou
School of Mechanical Engineering
Georgia Institute of Technology

Dr. Donggang Yao
School of Materials Science and Engineering
Georgia Institute of Technology

Date Approved: [April 25th, 2019]

ACKNOWLEDGEMENTS

I would like to express my deepest appreciation to my thesis advisor, Dr. Tequila A. L. Harris, who offered such great opportunity of work and then provided tremendous support and guidance through my entire graduate degree at Georgia Tech. I would also like to extend my deepest gratitude to Dr. Donggang Yao and Dr. Kyriaki Kalaitzidou for their all-time support in their specialty area during the project. The completion of my thesis study would not have been possible without the support and nurturing of the whole committee.

Special thanks to Dr. Hong Yeo, who generously provided me with the Aerosol Jet Printer access and training. I gratefully acknowledge the effort of the IEN staff, especially Walter Henderson, Eric Woods, and Rebhadevi Monikandan, for supporting my material characterization needs as best as they could. Additionally, I'd like to acknowledge the MILL staff for assistance on several different instruments. I would also like to thank my research group members, Ara Parsekian, Tae Joong Jeong, Jesse Sesito, and Peter Griffith for providing thorough training and sharing abundant technical knowledge with me. I also wish to thank all the instructors, lab mates, and friends I encountered who made my life at Georgia Tech so meaningful and unforgettable.

Finally, I'm extremely grateful to my parents and my entire family, without whom I would not have had the opportunity to study in United State at Georgia Tech. I would like to thank them for their unconditional love, companionship, and the greatest support since I was born.

TABLE OF CONTENTS

ACKNOWLEDGEMENTS	iii
LIST OF TABLES	vi
LIST OF FIGURES	vii
LIST OF SYMBOLS AND ABBREVIATIONS	ix
SUMMARY	x
CHAPTER 1. INTRODUCTION	1
1.1 Background and Its Significance	1
1.2 Existing Technologies and Challenges for Fabricating Silk Fibroin	2
1.3 Thesis Overview	4
1.4 Thesis Organization	5
CHAPTER 2. EXPERIMENTAL METHODS	6
2.1 Regenerated Silk Fibroin Solution Procedure	8
2.1.1 Degumming	8
2.1.2 Dissolution	11
2.1.3 Dialysis	11
2.1.4 Centrifugation	11
2.2 Material Fabrication on Aerosol Jet Printer	12
2.2.1 Printing Method	13
2.2.2 Varying Process Parameters and Post-Processing for the Investigation	15
CHAPTER 3. RESULTS AND DISCUSSION	17
3.1 Material Preparation and Characterization	17
3.1.1 Degumming	17
3.1.2 Dissolution	17
3.1.3 Dialysis	18
3.1.4 Material Preparation Protocol	19
3.1.5 Contact Angle and Strength	20
3.2 Material Fabrication	21
3.2.1 Feasibility of Printing at Various Dialysis Times	21
3.2.2 Qualifying AJP defects	22
3.2.3 Comprehend Various Regimes in Operating Window	26
3.2.4 System Drift	30
3.3 Overspray Phenomena	31
3.4 Effect of Surfactant (Triton x-100) on Printed Pattern	34
3.4.1 Impact of Triton on Pattern Composition	35
3.4.2 Impact of Triton on Pattern Geometry	37
3.5 Effect of Focus Ratio on Printed Pattern	40
3.5.1 Impact of Focus Ratio on Pattern Geometry	41
3.5.2 Impact of Focus Ratio on Overspray	46

3.6	Challenges	48
3.7	Summary	51
CHAPTER 4.	CONCLUSION	52
CHAPTER 5.	FUTURE WORK	54
REFERENCES		56

LIST OF TABLES

Table 1	Modified material preparation protocol [24]	20
Table 2	Different dialysis time for ink rate of 20 sccm	22
Table 3	Quality criteria for RSF printed patterns	24
Table 4	Summarized process variables for entire experiment	25

LIST OF FIGURES

Figure 1	Flow chart for the entire experiment	7
Figure 2	Transition from silk cocoon to RSF solution	8
Figure 3	Modified protocol for aerosol jet printable RSF solution	10
Figure 4	Transition from RSF solution to printed pattern	12
Figure 5	(a) AJP schematic and (b) the focused beam captured when printing RSF.	14
Figure 6	Operating window for 48 hr dialysis RSF solution	26
Figure 7	(a) Pooling of circle (b) Circle without pooling (c) Mahajan et al.'s work on ill-defined edge(scale bar=50 μ m) [29] (d) Pooling of line (e) Line without pooling	28
Figure 8	Raman spectra for prints with representative morphology	30
Figure 9	Repeated operating window with 48hr-dialysis RSF solution	31
Figure 10	Overspray Phenomena (a) Overspray of silver nanoparticle (Mahajan et al's) (b) SEM image of RSF overspray (c) Leica optical microscope image of RSF overspray	32
Figure 11	EDS Elemental Analysis (a) Raw cocoon (b) Degummed cocoon (c) LiBr (d) Edge of printed pattern and (e) Center of printed pattern	33
Figure 12	Pattern deposition (a) before and (b) after adding Triton	35
Figure 13	(a)Full range Raman spectra (b) Selected region for Raman analysis (c) After linear combination	37
Figure 14	3D image of pattern without(a) and with(b) Triton	39
Figure 15	Relationship between line width and focus ration as a function of ink rate for RSF solution with and without Triton	40
Figure 16	Optical images for the influence of process parameters on line morphology	43
Figure 17	Circle pattern with increasing FR at ink rate of 23 sccm	43

Figure 18	Influence of focus ratio (FR) on line width (a) all with Triton and (b) all on same run	45
Figure 19	Influence of focus ratio (FR) on pattern thickness	46
Figure 20	(a) Overspray definition. (b) Influence of focus ratio (FR) on overspray	48
Figure 21	(a) Cross-sectional view of RSF on copper substrate (b) Cross-sectional view of RSF on copper substrate showing the concavity	50

LIST OF SYMBOLS AND ABBREVIATIONS

AJP	Aerosol Jet Printer
IJP	Ink Jet Printer
RSF	Regenerated Silk Fibroin
DOD	Drop On Demand
FR	Focus Ratio
Triton	Triton X-100
SEM	Scanning Electron Microscope
EDS	Energy-dispersive X-ray Spectroscopy
PPT	Parts per Thousand
NEA	Norland Electronic Adhesives
OS	Overspray
TGA	Thermogravimetric Analysis

SUMMARY

Regenerated silk fibroin (RSF) solutions have gained a lot of attention due to its strong mechanical properties, biocompatibility and biodegradability. To exploit these unique properties, for applications such as drug delivery, packaging, biosensor, and wound treatment non-contact, maskless printing methods are highly desirable, such as inkjet printing (IJP). However, IJP is prone to clogging and typically additives, which alter the chemistry of the solution, are required to successful deposition. In this work, a framework for using aerosol jet printer (AJP) to fabricate RSF solutions derived from cocoons of the silkworm is developed. A unique combination of degumming, dissolving and dialysis conditions is required to prepare an aerosol jet printable RSF solution. It has been found that slight changes in those steps can lead to gelation or printing defects. Even so, it has been shown that additives are not required for AJP RSF solutions, and when added have a negative impact on the printed pattern. From the developed operating window, it has been shown that outside the optimum ranges, the patterns will be subjected to several defects including discontinuities, pooling and cloudiness. An artifact of AJP known as overspray has been found to be an uncontrolled phenomenon that can be reduced by increasing sheath rate. The results of this investigation introduce the feasibility of AJP patterns from RSF solutions.

CHAPTER 1. INTRODUCTION

1.1 Background and Its Significance

Silk fibroin produced by silkworms has been used commercially as biomedical sutures for centuries, due to its unique combination of mechanical properties, biocompatibility, and biodegradability. More recently, research is being conducted on regenerated silk fibroin (RSF) solutions to understand the various forms the material can be fabricated into such as films, coatings, sponges, and nanofibers, to exploit these unique properties for applications, such as drug delivery, packaging, biosensor, and wound treatment [1, 4-8]. These biomaterials have been found to be a better alternative to other synthetic polymers or copolymers. For instance, due to its low inflammatory response and similar permeability and diffusivity, silk fibroin has been found to have great potential for controlled release [2]. Anticancer drugs, small molecules, and biomolecules with higher biocompatibility and biodegradability have been used in drug delivery systems that perform better than poly(lactic-co-glycolic acid), PLGA, a commonly used copolymer [3] in food packaging industry. Odorless silk fibroin coatings have prolonged the freshness and firmness of fruit, due to its porosity and biodegradability [4]. Silk fibroins have also been shown to accelerate wound healing compared with commercially available products in both animal models and clinical trials [5]. From the perspective of microscale applications, layer-by-layer fabricated capsules, drug delivery of microparticles or nanoparticles, scaffolds for tissue microenvironment, and biosensors like optical waveguides all benefit from materials with similar properties of silk fibroin, which must be fabricated with high resolutions [6-8]. Tao et al. have

shown RSF added to biological dopants, such as enzymes, growth factors, or any other biological compounds, have much less biological activities when compared to being stored or inkjet printed (IJP) with water based solutions. For these biomaterials, additive manufacturing techniques rather than conventional techniques for microfabrication purposes are considered more efficient production process, higher volume throughput, and sustainability in the long run [9]. To this end, bioprinting of burgeoning materials such as functionalized silk fibroin is a crucial and important research area especially as it relates to printing at the microscale or lower [10].

1.2 Existing Technologies and Challenges for Fabricating Silk Fibroin

Techniques that have been utilized to fabricate silk fibroin mainly include lithographic related approaches and direct-write printing beyond the conventional approach of spinning or casting [11]. The traditional lithographic related methods require stamp removal, which leads to a considerable amount of waste. Furthermore, this subtractive method involves multiple manufacturing steps that can cause more human error and energy waste [12]. Multiphoton lithography is able to scale the patterns down to 100 nm. However, the process uses a laser, photoinitiator dye, and other chemical additives that adversely affect the properties of the silk fibroin [11]. The emergence of direct-write printing, an additive technology that uses computer-aided design (CAD) software to specify the geometric features of the printed patterns, has been shown to overcome some of the weaknesses of lithography [13]. There are four categories of direct-write printing – flow-based direct write, energy beam based direct write, tip-based direct write, and droplet based direct write. Inkjet and aerosol jet are droplet based direct write methods that have unique characteristics, making them more amenable for

processing materials such as silk fibroin solutions [13]. Both of these two techniques are non-contact, maskless, scalable, and have a resolution of 10 μ m. To date, inkjet printing (IJP) is a more broadly accepted approach due to its maturity and ubiquity in both industrial and commercial applications [14]. There are two types of IJP, drop-on-demand (DOD) and continuous. DOD is more popular because it eliminates complicated steps involved in continuous inkjet printing, such as recycling unused functional inks, which can have a major impact on their properties [15]. In the case of DOD systems, the piezoelectric-based inkjet is more commercially accepted than a thermal-based inkjet due to the fact that it processes the material without generating the thermal effect, which can damage the labile chemical compounds in the ink [10]. An alternative non-contact IJP fabrication method has emerged, named electrohydrodynamic printing. It has a higher resolution than other methods at several hundred nanometers. Hashimdeen et al. were able to achieve the highest resolution for printed silk fibroin reported, 1 to 2 μ m using electrohydrodynamic printing by altering the print head design. The higher resolution of this technology is mainly because of the large jet diameter to nozzle diameter ratio, which at the same time brings the drawback of jet instability, thus creating limitations for this technique [16].

Currently, a major challenge for printing silk fibroin is its low printability. For improved printability, RSF solutions must be mixed with other polymers [17]. There are three main reasons, which cause extremely low printability of silk fibroin. First, the micro-nozzle head is frequently clogged due to the β -sheet crystallization induced by shear stress during printing. Second, reduced mobility of macromolecular and shear thinning of the silk fibroin at high or low concentrations limit the concentration range that

produce an optimal printing condition. Third, random degradation incurred during the degumming or dissolution step is hard to control, which can have a large impact on the ink viscosity [17]. Typically, DOD inkjet printing is only able to process inks in the viscosity range of 10-40 cP [18]. Therefore, researchers often use viscosity modifiers to adapt the functional ink to the printing environment, such as increasing the viscosity of dilute solutions to increase printability. However, it has been reported that protein, e.g., silk fibroins, can have a scenario where viscosity inhibits the printability [19]. Although increasing the viscosity may lead to higher printability or finer resolution [20], it will decrease cell viability and solution stability, which can accelerate the gelation time of the RSF solution [21]. These are roadblocks for using RSFs in the cell manufacturing industry [22].

1.3 Thesis Overview

With all the disadvantages and challenges of printing RSF summarized above, the objective of this work is to demonstrate that there exists a pathway to Aerosol Jet® print (AJP) regenerated silk fibroin solutions without additives or clogging the nozzle. AJP is an emerging additive manufacturing technology that is capable of producing a very small drop volumes (60 fl), compared to common inkjet printers (60 pl), which can significantly reduce the feature size [23]. This innovative technique allows for processing a wide range of viscosities from 1 to 1000 cP with a working distance of up to 5 mm. In this work, a new processing method for RSF is introduced which includes three critical process steps (degumming, dissolution, and dialysis) to formulate RSF solutions that can be aerosol jet printed. Then the RSF solution is used to develop an operating window whereby the processing parameters (sheath rate and ink rate which forms the focus ratio

(FR)) are compared to the morphology of printed patterns to determine the best conditions for processing high quality uniform and defect free thin films. This work is applicable for fabricating RSF thin films across multiple scales, e.g., macro- and micro, using an innovative bottom-up, scalable manufacturing process, AJP.

1.4 Thesis Organization

Chapter 1 is intended to give a brief introduction of this thesis work, explaining the background and significance of this work by summarizing the advantages of RSF over other material and the roadblocks of existing competing technologies. Chapter 2 outlines the necessary steps for formulating such AJP printable RSF solution and also presents a visual friendly flow chart and schematic for better understanding the entire experimental setup. In Chapter 3, the modified protocol is explained with several important notes for making the RSF solution aerosol jet printable. In addition, an operating window is developed to present the boundary limits of AJP RSF solutions, while giving consideration to not only processing defects but also system drift. The effect of surfactant and focus ratio (FR) on the pattern geometry is also investigated. Chapter 4 summarizes the important findings in this thesis with the future work listed in Chapter 5.

CHAPTER 2. EXPERIMENTAL METHODS

The flow chart shown in Figure 1 explains the experimental flow of this thesis, which can be broken down to two main parts, *material preparation* of RSF solutions and *material fabrication* of RSF thin film using AJP. This chart is composed of several loops, which provides corresponding steps in the case of unwanted phenomenon, such as formation of gel during one of the last steps of material preparation or during the atomization of the AJP, as well as pooling during the AJP tuning processes. The material preparation consists of four steps, degumming, dissolution, dialysis and centrifugation. The material fabrication consists of two steps, atomization and tuning parameters before actually moving on to printing.

There is a delicate balance that much be maintained between the materials preparation steps and the material fabrication steps in order for the solution to be printable. Each batch of solution formed using the material preparation procedure produces around 5 ml of purified RSF solution. However, mistakes during the first two steps of the materials preparation stage cause gelation before or during AJP atomization, rendering the solution unprintable [17]. This only happens if the material preparation protocol is not strictly followed, otherwise trial and error needs to be implemented if it still turns to gel. If *gelation* occurs before or during AJP atomization, it suggests the degumming time is shorted than desired. Thus, the batch of solution is discarded and a new batch is made using increased degumming time, by up to 15 min in 5 min intervals. If *pooling* occurs while tuning the AJP, the batch of RSF solution is deemed unprintable and is discarded because this suggests the degumming time is longer than desired. A new

batch of RSF solution is prepared by decreasing the degumming time by up to 15 min in 5 min intervals. For either case where the solution must be remade, decreasing the ratio of silk fibers to deionized (DI) water can lead to more uniform degumming.

After successfully tuning the AJP and printing patterns, the samples are post-processed and the morphology and geometric features are analyzed. In order to ensure the consistency among the experiments, the aforementioned processes must be repeated, starting from the dried white silk step illustrated in Figure 1, for each AJP run because the RSF solution can become unstable due to temperature, humidity, time stored, and solution concentration [21].

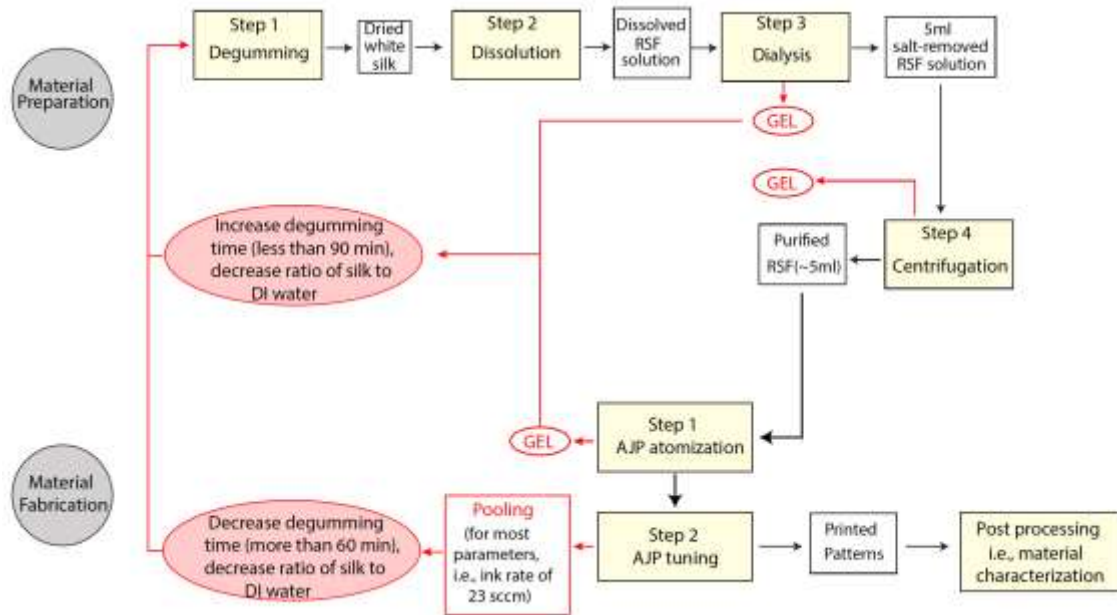


Figure 1. Flow chart for the entire experiment

2.1 Regenerated Silk Fibroin Solution Procedure

RSF solutions with silk concentrations between 2.7% and 5.7% and dialysis time between 3 hr and 48 hr are prepared for this study, using the four steps outlined in Figure 1, degumming, dissolution, dialysis, and centrifugation in order to process such silk cocoon into RSF solution. Although the steps are standard [24], modifications have to be made in order to formulate aerosol jet printable solutions, as illustrated in Figure 2, that will not gel or pool.

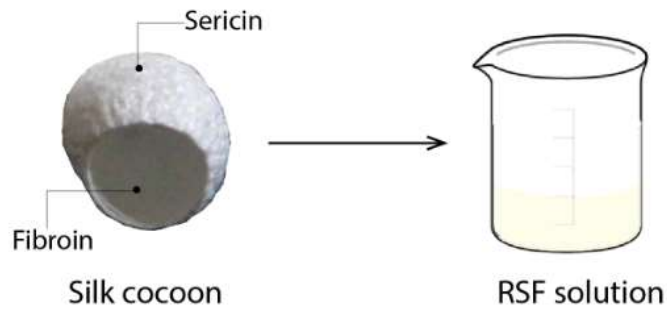


Figure 2. Transition from silk cocoon to RSF solution

2.1.1 Degumming

Silk fibroin, which is found in the cocoon of the silk worm, is highly desirable for its combination of attractive mechanical properties and biocompatibility. Silk protein is identified as the major component of silk cocoon, including 70%-80% silk fibroin and 20%-30% sericin, with sericin being the rigid gum shell of silk fibroin as the structural center [25]. The silk fibroin is obtained by removing sericin, shown in Figure 2, from the cocoon architecture, with the sericin being reported as bio-incompatible [1]. The process

of removing the sericin is called degumming [26]. The steps involved in degumming include cleaning, boiling, and drying.

Cocoons, 15-20 g, are cleaned and cut into quarters to increase the exposed surface area during degumming. This solution is prepared by adding 0.02 M sodium carbonate to 2.5 L DI water to form a 0.212% wt/vol aqueous solution. The cocoons are then added to boiled sodium carbonate solution at 100°C, while constant stirring, for 75 min, to form fibrous solids. For the purpose of consistency and accuracy, the fibrous solid is kept in oven for 24 hr with a cover at 80°C after being rinsed 3 times in order to be fully dry. It may be fully dry around 20 hr depending on how much water is squeezed out before it is placed into oven. Thus, multiple checks after a whole night of oven drying is necessary to avoid over heating of the fibrous solid.

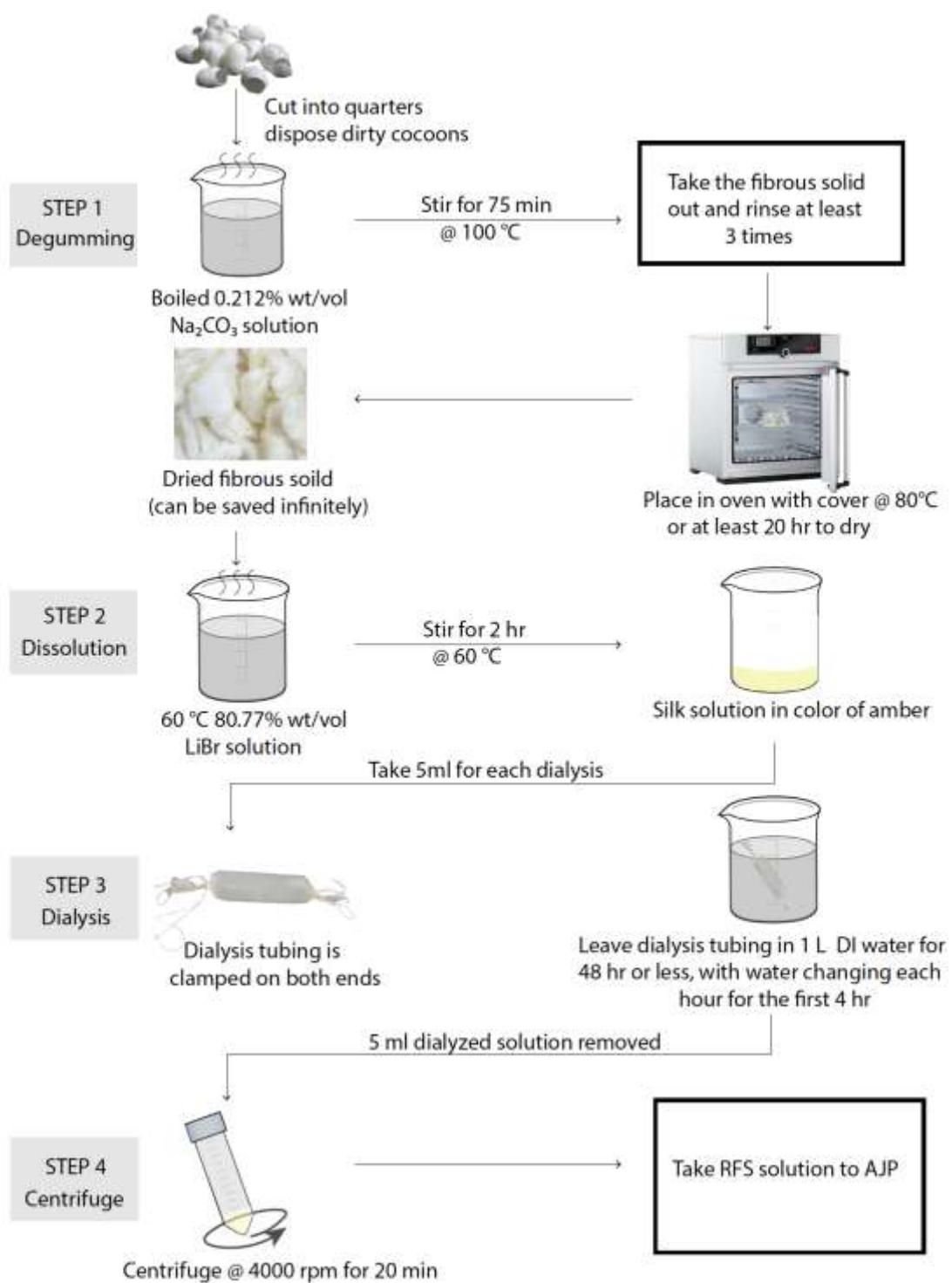


Figure 3. Modified protocol for aerosol jet printable RSF solution

2.1.2 Dissolution

After drying the degummed fibers, lithium bromide, Anhydrous 99% min, was used to make 100 ml of 80.77% lithium bromide solution (9.3 M LiBr) to dissolve the fibrous solid. This process is conducted at 60°C with magnetic stirrer for 2 hours on hotplate. Fibrous solid with mass of 3.5 g, 7 g, and 13 g are tested respectively for the purpose of understanding an optimal protocol for aerosol jet printable solutions. The fibrous solids are added in small amounts (~0.5 g) for more effective dissolution with manual stirring [24]. Once fully dissolved within 1.5 - 2 hr, the RSF solution is cooled and dialyzed or stored in the refrigerator at around 4°C to analyze the physical property viscosity or salinity later.

2.1.3 Dialysis

A portion of the solution from the dissolution step, 5 ml, is dialyzed in DI water with a 1:200 ratio to wash out LiBr, which is utilized to dissolve the silk fibroin. Dialysis membrane tubing (obtained from VWR) is soaked in DI water for at least 3 seconds to easily open it. The tubing is filled with 5 ml RSF solution with both ends carefully clamped. The tubing is clamped and placed in 1 L of DI water. For the duration of the dialysis step, the tubing remains clamped. The DI water is changed every hour for the first 4 hours. After the first four hours of changing the DI water, the solution within the dialysis tubing is monitored every 12 hr for an additional 44 hr. Hence, the dialysis step takes 48 hours.

2.1.4 Centrifugation

All solutions are centrifuged in centrifuge tubes, obtained from VWR. The centrifuge occurs at 4,500 rpm under 4°C for 20 min, the centrifugation process is repeated if impurities are found in the solution after the initial centrifuge process. As stated previously, if gelation occurs by the end of centrifugation, the batch is discarded and the procedures of degumming and dissolution are repeated according to the troubleshooting steps provided in Figure 1.

2.2 Material Fabrication on Aerosol Jet Printer

There is a 3-step approach using AJP for fabricating RSF solutions into printed patterns, such as circle patterns, aiming for developing operating window, and line patterns, aiming for investigating relationships between process parameters, with the transition shown in Figure 4. The three steps include atomization, AJP tuning, and printing within the operating limits.

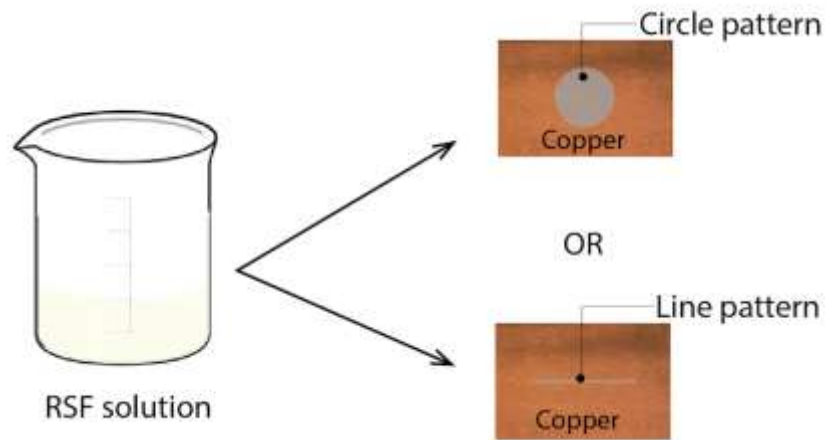


Figure 4. Transition from RSF solution to printed pattern

2.2.1 *Printing Method*

The AJP system used in this study is an Optomec Aerosol Jet 200[®]. As shown in Figure 5 (a), the two main components are the vial stored with printing ink and the deposition head, which is connected to the vial via a perfluoroalkoxy alkanes (PFA) tubing. Intuitively, the working principle for the system is that the ultrasonic atomizer creates aerosol of ink inside the vial, which is carried towards the deposition head by Nitrogen. In this study, the ultrasonic atomizer is designed for a lower viscosity range while the other pneumatic atomizer is designed for a higher viscosity range. Another Nitrogen source named sheath gas at deposition head generates a focused beam as the ink deposits onto the substrate. A focused beam when depositing RSF solution is captured in Figure 5 (b) with the shutter in the open position. AJP delivers a continuous stream of aerosols while printing with a shutter below. The shutter has a back and forth movement within 1 cm distance controlled by the software to pause the flow at designated locations where it is not supposed to be depositing. The aerosol can be defined as a suspension of fine solid particles or fine liquid droplets, leading to differences in pattern morphology. For each AJP run, 0.5 ml of silk fibroin solution is added to the vial for printing various patterns and cannot be reutilized after storage, unless otherwise noted. During the AJP process microdroplets of RSF rapidly solidify and collect on the shutter. Because of this, the shutter is cleaned with Acetone every 30 min.

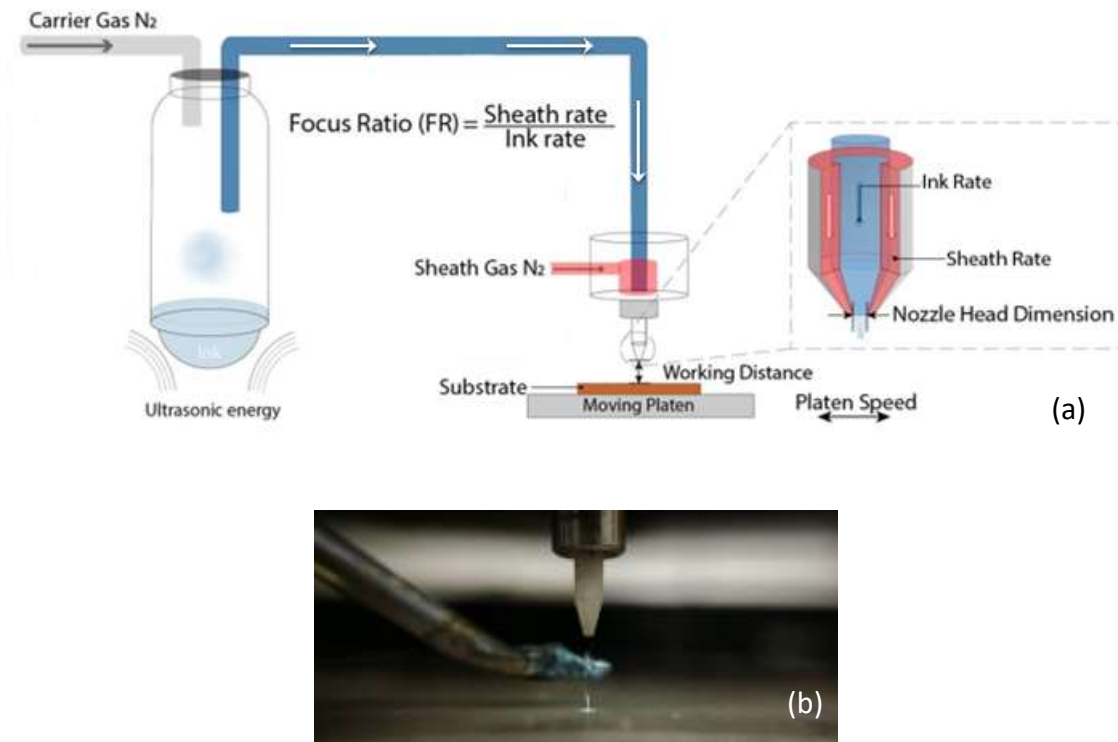


Figure 5. (a) AJP schematic and (b) the focused beam captured when printing RSF.

The substrate is copper foil laminated on a thin glass slide with no air bubble entrained to ensure flatness. The whole system, including vial support, tubing, deposition head, etc. is thoroughly cleaned using an ultrasonic bath and rinsed with Acetone before printing RSF solution to minimize contamination. A test pattern before and after printing is made to ensure stable and accurate equipment performance from the initial to the last print; this is considered AJP tuning. It has been demonstrated that there exists more significant system drift for silk fibroin than other metallic ink as Smith et al. being the first to discuss this phenomenon recently [27]. Thus, the test pattern (in the form of a line or circle) is deposited frequently on a spare substrate to ensure that it conforms with the criteria table discussed later in Section 3.2.2 to a large extent. For instance, several runs at different boundaries (regimes) of the operating window should be nearly the same

visually to ensure consistency between runs.

2.2.2 *Varying Process Parameters and Post-Processing for the Investigation*

There are two main process parameters for controlling the AJP, carrier gas flow rate and sheath gas flow rate. The carrier gas flow rate is also named atomizer or ink flow rate (ink rate) with a maximum range of 50 sccm (standard cubic centimeters per minute). This parameter controls the amount of mist generated from the atomization to the deposition head. The sheath gas flow rate (sheath rate) dictates the flow rate of the microdroplets deposited at the deposition head, between 20 to 150 sccm. The focus ratio (FR) is calculated from the following:

$$\text{Focus Ratio} = \frac{\text{Sheath gas flow rate}}{\text{Ink flow rate}}$$

is defined as the focus ratio, FR. The focus ratio is a critical factor for determining print quality. The process parameters would be written as (40,20) if the sheath rate is 40 sccm and the ink rate is 20 sccm. Other fixed parameters in this study are ink and platen temperature, which are set at 25°C, the selected nozzle head is 150 µm, working distance between the nozzle head and substrate is 3 mm, and the platen speed is set to 2 mm/sec.

Line and circle patterns are processed using the AJP. Line patterns are used to investigate the effect of focus ratio. Circle patterns are used to develop the operating window. Both line and circles patterns are utilized to understand the effect of overspray and subsequently surface treatments, e.g., adding surfactant (Triton X-100) to the solution.

A salinity refractometer from Aqueous Lab is used to measure the salinity of the

final solution before printing. Viscosity is measured, for solutions with different dialysis times, using RheoSense microVISCTM Viscometer. Leica DVM6 digital microscope, Hitachi SU8010 SEM and Phenom desktop SEM are used to capture the morphology of the samples, and then imageJ is used to measure various dimensions such as line width, circle inner and outer diameters. Zeta optical profiler is used to measure the thickness of the samples. Sample composition and the raw material datum are measured via the Phenom SEM with energy dispersive X-ray spectroscopy (EDS). Renishaw Raman Spectrometer is used to measure the Triton concentration in the patterns. Contact angle measurements are made using Rame-Hart goniometer 500U1.

CHAPTER 3. RESULTS AND DISCUSSION

3.1 Material Preparation and Characterization

In this section, the protocol for preparing the RSF solution is discussed. Modifications to the process are explained in relationship to mechanisms that influence them. Then the suggested process for preparing a solution that is aerosol jet printable is provided. Properties of the RSF solution made using the modified process are measured to ensure good wetting during material fabrication.

3.1.1 *Degumming*

The degumming time is a critical step in the material preparation step. The boiling time cannot exceed 90 min or the fibroin will degrade and cause pooling when AJ printing. Nor can it be shorter than 60 minutes since it will bring unwanted gelation before or during the AJP atomization. Relatively shorter time of degumming around 60 minutes may be able to produce RSF solution that neither turns to gel by the end of dialysis nor during the several trials of atomization on AJP.

3.1.2 *Dissolution*

With the repetitive steps that are done for producing fresh solution for AJP, the volume of the LiBr solution is scaled down to 50 ml or can be even smaller to reduce waste, since the rest of the dissolved silk solution is discarded in this experiment to ensure a fresh state of the silk fibroin solution for AJP. It takes 1.5 hr to dissolve 13 g of fibroin and only 20 min to dissolve 3.5 g of fibroin, by observation; however, continuously stirring at 60 C for a full 2 hours is necessary to completely dissolve the

solution. The dissolved solution is amber with some impurities, which are centrifuged out later. Dissolving 13 g of silk in dissolution step is proven to be too high in concentration (10.5%) with significantly lower solution stability since it turns to gel during the dialysis step even by the first 24 hour. A concentration around 6% or lower leads to printable and more stable solution.

3.1.3 Dialysis

Different time lengths for dialysis have been performed to better understand its effect on AJP of RSF solution. Traditionally, four days are required to produce 5 ml of RSF solution, with a dialysis time of 48 hr, which is relatively time-consuming. Viscosity and salinity measurements are conducted to understand their affect on the solution.

From the salinity measurements between 3 or 48 hr dialysis time ranges from 17 to 6 parts-per-thousand (ppt) which equates to 0.6 - 1.7%. Solutions that did not undergo dialysis are measured to 100 ppt or higher. The viscosity varies from 2.067 - 2.308 cP for RSF solution concentrations of 2.7% and 5.7%, respectively, for dialysis times of 3 or 48 hr. When the solution has not undergone dialysis, the average viscosity is measured to be 13.07 cp. It has been found that the viscosity decreases with increased dialysis time, which also leads to decreased salinity. The results of these two physical properties indicate that the first three hours of dialysis has a major impact on the physical properties of the RSF solution.

The remainder of the dialysis time plays a major role of setting the solution at a steady state. The solution should only be getting clearer as time passes by and turns out to be a clear solution like water in the end of 48 hr dialysis, instead of appearing to be half

transparent and half jelly during the process. If that occurs and is not observed, then the solution might fully turn to gel after 48 hr or after centrifugation or eventually during AJP atomization, which will only consume more non-value added time.

3.1.4 Material Preparation Protocol

A modified procedure for making the RSF solution has been developed, with changes to the degumming and dissolution times. The degumming time is increased by 45 min, however it ensures no gelation during AJP tuning and the dissolution time decreased by 2 hr. The dissolution method is more convenient but being as effective as the original protocol without the safety hazard of possible skin exposure to splashed hot LiBr solution compared with the method used by Rockwood. The ratio of RSF to DI water is decreased for a better dialysis outcome since 5 ml is sufficient for an AJP run. The modified procedure is shown in Table 1.

However, there are several indications showing that a batch of solution is of poor quality, such as gelation during dialysis, centrifuge, or AJP atomization. With these variants and all the environmental factors that RSF is sensitive to, this protocol is a guide to researchers. Some variations in protocol may have to be made when processing in different environments.

Table 1. Modified material preparation protocol [24]

Step	Critical Item	Rockwood et.al Protocol [24]	Modified protocol
Degumming	Na ₂ SO ₃ amount	0.02 M	0.212% wt/vol (0.02M)
	Boiling time	30 min	75 min
	Rinse	3 times each 20 min in ultrapure water with stir	3 times each 1 min in DI water
	Drying	In air 12 hr	Oven 80 °C 21~24 hr
Dissolution	LiBr amount	9.3 M	80.77% wt/vol (9.3 M)
	N/A	Add LiBr on top of silk, 4 hr	Add silk to LiBr solution, 2 hr
Dialysis	Volume	12 ml SF to 1 L ultrapure water	5 ml SF to 1 L DI water
	Water change	6 changes throughout the 48 hr period	4 changes each hour for the first 4 hr
	Time	48 hr	48 hr
Centrifuge	N/A	9000 rpm 4 °C 20 min twice	4500 rpm 4 °C 20 min
RSF Solution	Concentration	7-8% wt/vol	2.7%, 5.7% wt/vol

3.1.5 Contact Angle and Strength

Contact angle of the RSF solution on copper is 70°. Although the RSF solution will wet the copper, adhesion may be a problem. The RSF is dry cast into a 50 µm thin film to test the tensile properties using ASTM D882 for thin plastic sheeting. The tensile strength is 3.76 MPa with a degumming weight loss of slightly more than 30%, which agrees with other findings; for instance, Benjamin et al. reported RSF strength of 4.3 MPa with a degumming weight loss of about 29.4% [28]. Therefore, this result suggests that such material formulation method does not alter its mechanical properties.

3.2 Material Fabrication

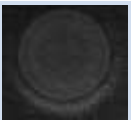

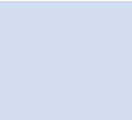



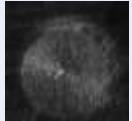

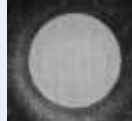



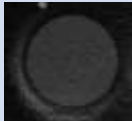
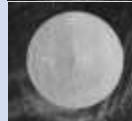


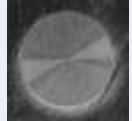








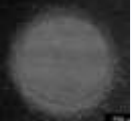
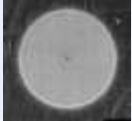


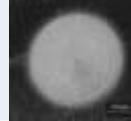
The feasibility of printing RSF solutions is investigated. In an effort to decrease the material preparation time, the effect of changing the dialysis time is analyzed first. Then, the coating window for RSF film is investigated using circles patterns for varying sheath and ink flow rates. In the past the influence of several different process parameters on the morphology of silver nanoparticles lines has been evaluated [24, 29], but this is the first such study for polymeric material. Defects such as pooling, non-focusing, or discontinuous lines, generated during the AJP process are qualified and are used to set the boundary limits of the operating window.

3.2.1 Feasibility of Printing at Various Dialysis Times

To study the sensitivity of dialysis time on pattern morphology, RSF solution is prepared using different dialysis times, 0 hr, 3 hr, 6 hr, 8 hr, 24 hr and 48 hr, with the aim of decreasing it as much as possible. Other material preparation parameters are kept constant. It is important to note that this study is not intended to show a comparison of print quality, under different dialysis time length, but rather the feasibility of aerosol jet printing the RSF solution. Because uncontrolled system shift, which outputs different pattern geometry under the same processing parameter at each time of running, limits the print quality and accuracy.

As shown in Table 2, dialysis is a requirement for aerosol jet printable RSF solution. Furthermore, it is shown that RSF solution with short dialysis time (3 hr) can produce the same quality of prints as 48 hr of dialysis. However, during AJP tuning it appears that there is much lower stability.

Table 2. Different dialysis time for ink rate of 20 sccm



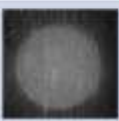







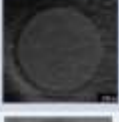

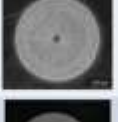







Dialysis Time(HR) Sheath rate(sccm)	48	24	8	6	3
120(FR=6)					
100(FR=5)					
80(FR=4)					
60(FR=3)					
40(FR=2)					
20(FR=1)					

3.2.2 Qualifying AJP defects

The AJP tuning process is a bottleneck of conducting experiments since from time to time troubleshooting is needed to obtain the same print quality achieved in a previous run, even if all procedures are exactly the same. System drift is the primary reason for this, although changes in the biomaterial may also be a factor. The flowcharts described in Chapter 2 can help determine the specific action that is required in terms of material preparation step. However, if the RSF solution is successful atomized, there may still exist occasions where the print quality is not consistent requiring further troubleshooting.

A visual guide for assessing print quality of AJP RSF solution is illustrated in Table 3. When tuning the AJP process, one or more of the conditions shown in Table 3 is used to illustrate consistency of the process. In Table 3, there are four grades for the print quality ranging from 1 – 4, 1 being the best and grading 4 being the worst, based on the defects. This table offers corresponding resolutions for improving the quality of a print from grades 3 or 4 to grade 1 or 2 for each criterion. These defects can be encountered during AJP tuning, i.e., within the optimum range, and thus do not necessarily occur at the boundaries of the operating window. For instance, the *ink not uniformly deposited* (e.g., discontinuous lines) can be improved by cleaning the tube or nozzle or by adding more ink. However, if it still occurs after repeating the suggested steps at the operating boundary, then it's the limitation of the AJP on the RSF solution. *Pooling of ink* in this case is slightly different from the pooling phenomena that set limits on the operating window, which is due to setting the ink rate to high relative to the sheath rate. Whereas in this case, when initially printing the RSF solution the pooling occurs due to excessive degumming time. Even so, this visual guide is used to help determine the operating window for AJP of RSF solution.

Table 3. Quality criteria for RSF printed patterns

Criteria	Grading 1 (Best)	Grading 2 (OK)	Grading 3 (Worse)	Grading 4 (Worst)	Troubleshooting Result
Cloudiness on or along the edge of pattern					Ultrasonic clean nozzle head for 15min
Skewed overspray					Replace and clean tubing, need to check nozzle.
Less ink deposited					Add more ink
Pooling of ink					Only occurs when degumming time is longer than it should be.
Ink not uniformly deposited					Clean tubing, nozzle, or add more ink

All experimental process variables are summarized in Table 4 to understand their interdependency and impact on printability. The variables for material preparation have limited interdependency. The squeezing step, during degumming, affects the drying time for the fibrous solid. There is interdependency between AJP tuning and operating window development. AJP atomization does not affect the AJP tuning process; however, the AJP tuning result affects the operating window, since the tuned printing condition dictates the baseline for the operating window. The impact to printability indicates the most critical variable throughout this experiment, being the degumming boiling time, fibrous solid amount, and dialysis time. Each of these determines the basic printability, RSF solution concentration, and solution stability during AJP fabrication. The first two steps of AJP fabrication exhibit the huge impacts to printability as well, as AJP

atomization suggests unprintable and AJP tuning implies some unprintable scenario along with some defects. When successfully tuned and printed within optimum conditions, none of the process variables have any impact to printability. The variables involved during material fabrication, such as sheath rate, ink rate, platen speed and temperature, working distance, and ink temperature, all have interdependencies with each other. However, the current study only focuses on controlling sheath and ink rate for optimum printing condition with the other process variables not fully studied on the interdependencies.

Table 4. Summarized process variables for entire experiment

	Process	Variables	Value	Interdependency (Y/N)	Impact to printability (Y/N)
Material Preparation	Degumming	Sodium Carbonate	0.212% wt/vol (0.02 M)	N	N
		Boiling Time	75 min	N	Y
		Rinse	3 times each 1 min in DI water	N	N
		Squeeze	N/A	Y	N
		Drying	Oven drying @ 80 °C 21 ~ 24 hr	Y	N
	Dissolution	Lithium Bromide	80.77% wt/vol (9.3 M)	N/A	N/A
		Dried fibrous solid amount	3.3 g or 7 g	N	Y
		Method	Add silk to LiBr solution till completely dissolved	N	N
		Stirring time	2 hr	N	N
	Dialysis	Volume	5 ml silk solution to 1 L DI water	N	N
		Water change	4 changes each hour for the first 4 hr	N	N
		Time	48 hr	N	Y
	Centrifuge	Setting	4500 rpm @ 4 °C for 20 min	N	N
Material Fabrication	AJP atomization	RSF solution	N/A	N	Y
	AJP tuning	Printed pattern	N/A	Y	Y
	Printing at optimum condition	Sheath rate	69 sccm	Y	N
		Ink rate	23 sccm	Y	N
		Platen speed	2 mm/s	Y	N
		Work distance	3 mm	Y	N
		Platen temperature	25 °C	Y	N
		Ink temperature	25 °C	Y	N/A

3.2.3 Comprehend Various Regimes in Operating Window

The graph shown in Figure 6 illustrates the operating window as a function of sheath rate and ink rate for RSF solution with a dialysis time of 48 hr. In this plot, ink rate is controlled in a range from 20 to 27 sccm and the sheath rate varying from 20 to 150 sccm, which makes the FR change from 1 to 6 with a step size of 1. This range of process parameters roughly applies to all RSF solutions no matter what the printed patterns are, how long the dialysis time is, and if surfactant is added or not. In the graph, the operating boundaries for patterns printed with the same FR are connected via different color lines. The optimum regime is found to be within an ink rate range of 23 to 25 sccm with a focus ratio between 3 to 4, which agrees with the trend observed when processing line patterns where the smallest feature size and most reduced overspray arise with an ink rate of 23 sccm.

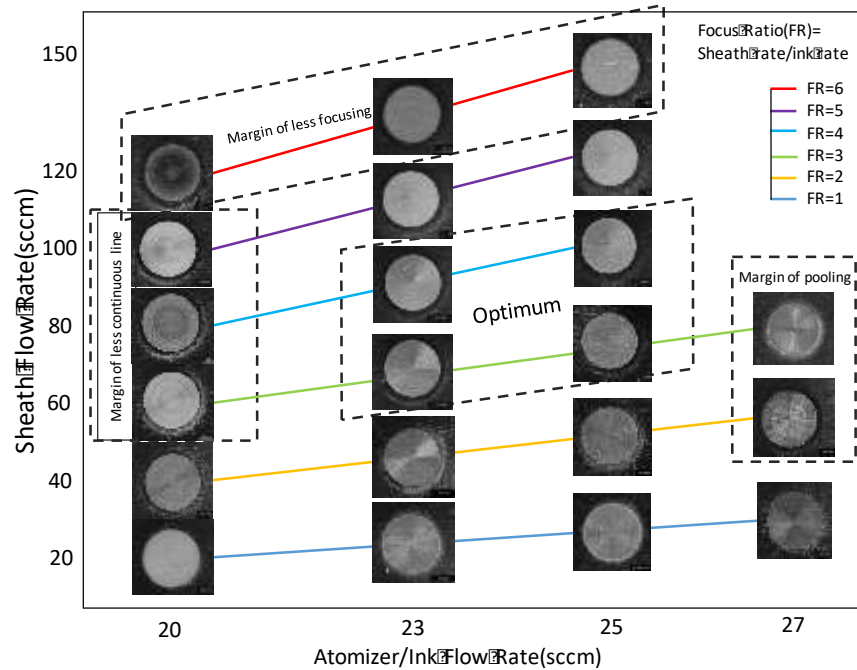


Figure 6. Operating window for 48 hr dialysis RSF solution

The margins or boundary limits are imposed based on the relationship between the sheath rate and the ink rate. Discontinuous prints occur when the ink rate is too low relative to the sheath rate, when the AJP deposits fine solid particles. It can be resolved by following the steps outlined in Table 3 if it is not close to the boundary limits, or by sampling increasing the ink rate. As FR increases at low ink rate, the boundary of discontinuous prints shows up and then gradually intersects the upper regime of the operating window where poor focusing occurs. The poor focusing regime occurs when the sheath rate is relatively high compared to the ink rate, e.g., FR of 5 or 6, because the high flow of gas at the nozzle tip deviates the RSF ink from its normal flow properties, leading to the cloudiness on top of the pattern or along the edge. To fix this issue, again, following the steps described in Table 3 can be done as well as reducing the sheath rate. It is important to note that the AJP nozzle is prone to clogging after either running for more than 1 or 2 hours. At the rightmost boundary, pooling occurs, because the ink rate is relatively high compared to the sheath rate, thus an excessive amount of fluid is dispensed onto the surface. In this case fine solid particles at the other margin can become coarse liquid micro droplets with more and more ink being deposited after the fine liquid micro droplets leading to the defect of pooling. Pooling for line and circle patterns of RSF solution are captured in Figures 7 (a and d) and without pooling in Figure 7 (b and e). The pooling phenomenon is very similar to the appearance to the ill-defined edges mentioned in Mahajan et al.'s work, shown in Figure 7 (c) which exists for all FR with a stage speed under roughly 3.8 mm/s [29]. The most noticeable difference between pooling phenomenon and fine liquid droplets deposited at high ink rate is illustrated in Figures 7 (d and e); however, neither of these results are due to excessive degumming

time. The main visual difference is that Figure 7 (d) shows an ill-defined edge while Figure 7 (e) shows more liquid state of line morphology but with a very sharp and clear-defined edge. Thus as seen in Figure 7 (a), the paths of the ill-defined edge coalesce into multiple pools, which deteriorates the final circle morphology, because when printing the circle using a perimeter it is filled gradually from the outer perimeter to the inner center point. The morphology, fine solid particles, near the left margin of the operating window, is captured in Figure 7 (b). Thus, it is rather intuitive to conclude that process parameters that can produce fine liquid droplets without pooling is the optimum operating window.

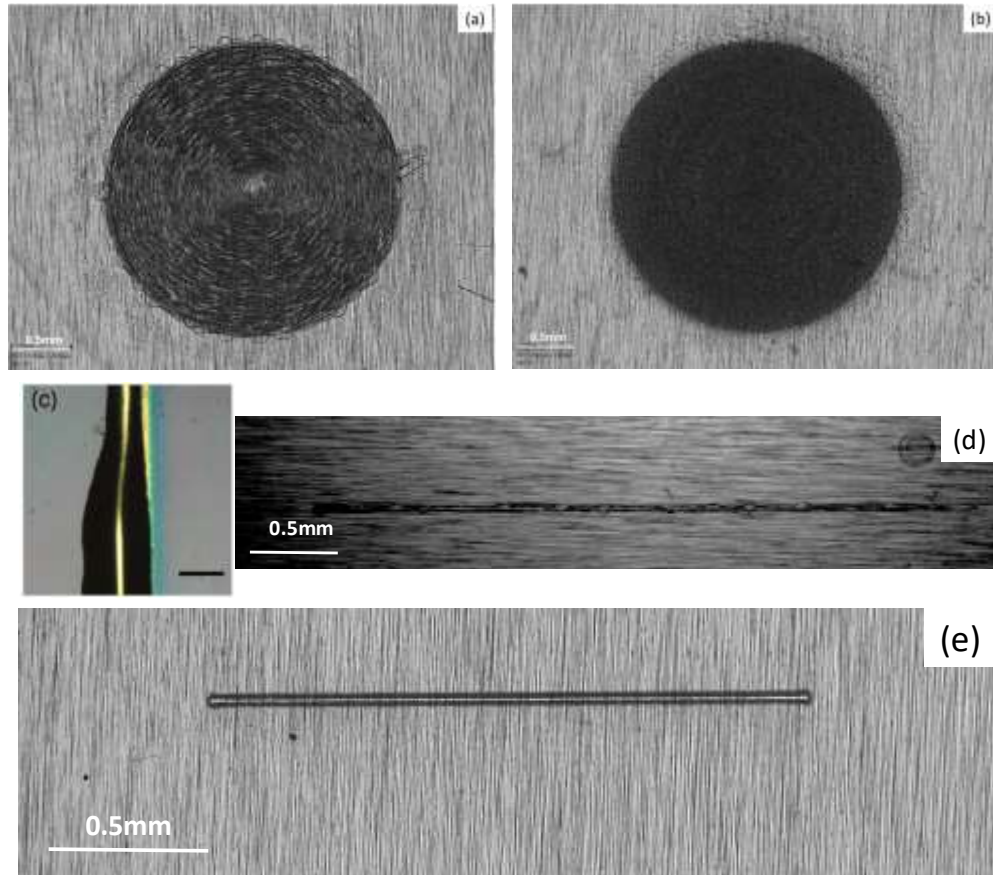


Figure 7. (a) Pooling of circle (b) Circle without pooling (c) Mahajan et al.'s work on ill-defined edge(scale bar=50 μ m) [29] (d) Pooling of line (e) Line without pooling

To understand the discontinuous patterns and patterns that exhibit pooling as shown at the left and right boundary in Figure 6, the patterns composed of fine solid particles and patterns composed of more liquid droplets are investigated using Raman spectroscopy. The Reinshaw Raman Spectrometer is used to analyze the chemical and structural information of the RSF patterns, because it is more sensitive than EDS and it is a contact free approach. From Figure 8 it is seen that the strongest peaks exist between 2,900 – 3,000 Raman shift-cm. Even though most of analysis is done at the Raman shift-cm of 1,650 for silk fibroin by other researchers, Raman shift-cm of 3,000 appears to be the best location for identifying material differentiation due to the unique form of the peaks across datasets. Since each sample has its own unique topology under different process parameters, the Raman scattering intensities are different for the same Raman scanning settings; hence the Raman shifts at main peaks are compared instead of their counts. Samples with fine liquid droplets at (25,25), with fine solid particles at (20,20), and with pooling phenomena at (30,30), are compared, because they represent the three main forms of printed RSF. These are then compared with the RSF datum for a droplet of pure RSF solution. Based on the Raman spectra, shown in Figure 8, solid particle and liquid micro droplets are merely an alternative structure of the deposited RSF solution, which does not affect the property since the spectra for the patterns align with the RSF liquid droplet.

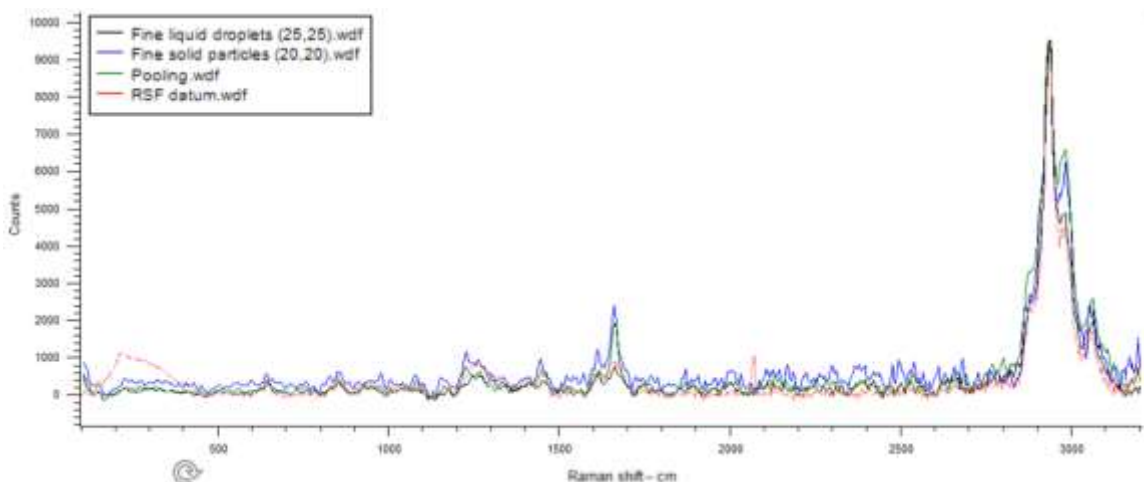


Figure 8. Raman spectra for prints with representative morphology

3.2.4 System Drift

The operating window for another batch of RSF solution with the same preparation protocol is shown in Figure 9. All procedures related in the experimental design remain the same, including the fixed operating parameters. Comparing Figures 6 and 9, it is clear that the operating window shifts to the left, e.g., the boundary of discontinuous patterns is removed from the visible boundary and the pooling phenomena shifts slightly. To this end, an ink rate between 20 and 23 sccm or FR from 3 to 4 are found to be the optimum range for printing. As the sheath rate increases at an ink rate of 25 sccm, the limit of the AJP for printing is reached. Although similar trends are observed, i.e., pooling at the right boundary, discontinuous patterns at the left boundary and overspray at the top and bottom boundaries, the reason for the system drift is not yet understood.

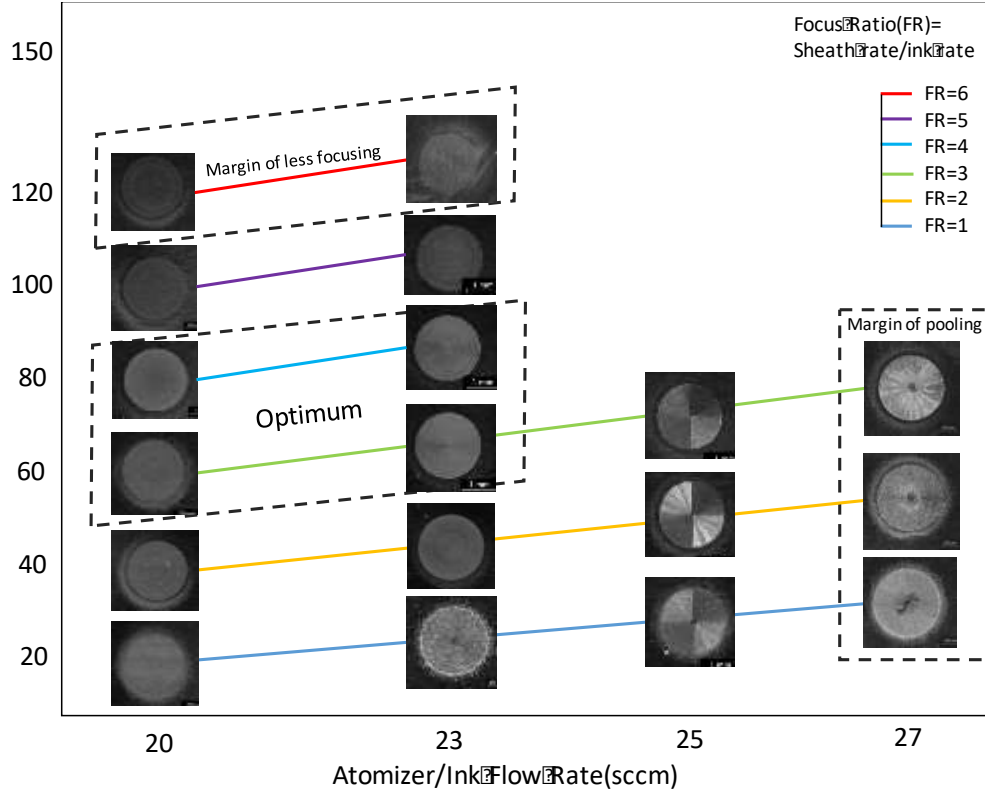


Figure 9. Repeated operating window with 48hr-dialysis RSF solution

There are several factors that affect the AJP experiments when fabricating the RSF solution. Two main factors are the machine and RSF solution. For example, the quality of the RSF solution can change over different batches, so a better process for quantifying the quality of the solution is needed. The machine can be challenging to calibrate resulting in system drift. Fortunately, the operating window, summarized trend, and comprehension of different pattern morphology in this thesis work provide a genuine guideline for researchers in this field.

3.3 Overspray Phenomena

Overspray, defined as the collection of aerosol droplets of aerosols that deviate from the expected pattern area, affects the spatial resolution significantly by increasing

the geometric features of the pattern, leaving the edges fuzzy and ill-defined. Overspray is very common for both AJP and IJP and for a variety of materials, and can be observed from the operating window from last section. Overspray of AJP silver nanoparticle and silk fibroin (RSF) are shown in Figures 10 (a and b). As shown, the two materials have similar morphology. The overspray can increase the feature size by twice of the actual width. Therefore, being able to minimize it significantly improves the quality of the printed pattern. However, it should be noted that the mechanisms, which influence overspray, are not well understood by researchers [29], and warrants.

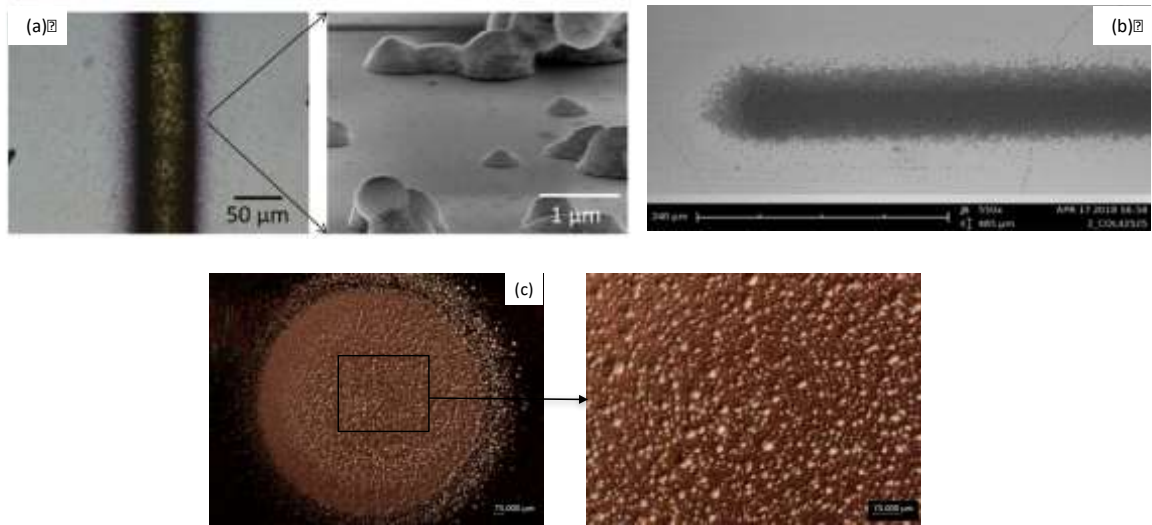


Figure 10. Overspray Phenomena (a) Overspray of silver nanoparticle (Mahajan et al's) (b) SEM image of RSF overspray (c) Leica optical microscope image of RSF overspray

The effect of LiBr (salt) content on overspray is investigated. Although the salinity test shows up to 1.7% of salt remaining in the solution, it is believed that the leftover LiBr may lead to the overspray along the edge of pattern. EDS analysis is conducted on raw cocoon, degummed cocoon, bulk Lithium Bromide, and printed patterns to understand the composition at each stage, as illustrated in Figure 11. As shown in Figure 11 (b), the degummed cocoon has slightly more nitrogen and less carbon if compared by

element weight concentration. From Figures 11 (d) and 11 (e), it is evident that LiBr is not on the edge or the center of the circle pattern tested. Comparing Figures 11 (b) and 11 (e), it is evident that the weight concentration of each element has only changed within 0.5% after going through the material preparation steps and AJP fabrication, which suggests that the whole process takes place without any unexpected chemical or physical reactions.

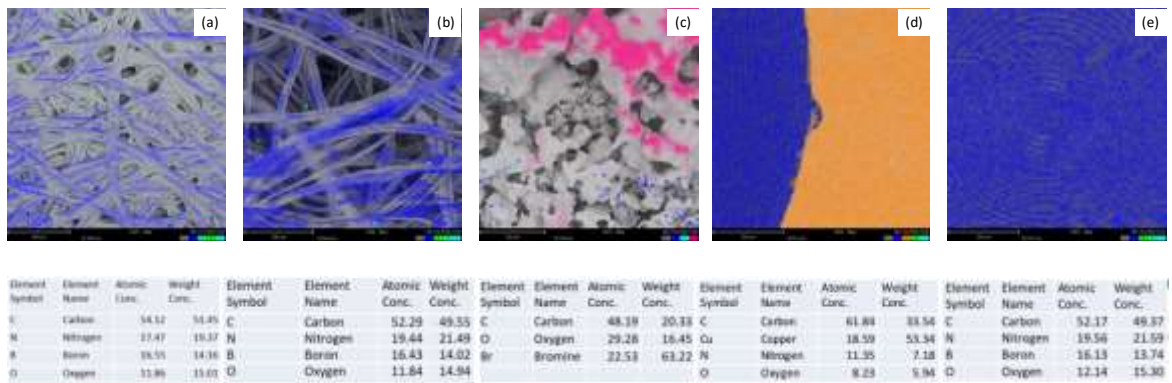


Figure 11. EDS Elemental Analysis (a) Raw cocoon (b) Degummed cocoon (c) LiBr (d) Edge of printed pattern and (e) Center of printed pattern

From the circular pattern shown in Figure 10 (c), large agglomerations of overspray droplets can reside not only on the perimeter but also on the top surface of a pattern. This is because AJP is set up to use a perimeter fill method when processing RSF solution; thus, with every pass the nozzle head moves closer to the center point allowing the overspray to be transferred to the surfaces of the patterns after each pass. This explains why there exists overspray both on and along the pattern. Smith et al. have indicated that the application of ultrasonic waves to the macromolecular solution can lead to the aggregation and gelation to some degree, which decreases the printability and has always

been a challenge for printing inks and solutions such as RSF solution [24]. The above indicates that overspray will not only affect the feature size from the geometry standpoint, but the quality of the pattern itself as well due to the agglomeration of particles that causes surface roughness. Adding surfactant has been shown to help with ink dispersion, preventing agglomeration, reducing ink evaporation, or adjusting ink rheological properties, which all contribute to printability [10, 30].

3.4 Effect of Surfactant (Triton x-100) on Printed Pattern

Different types of surfactants have been shown to enhance the mechanical properties of silk fibroin applications with maintaining its biocompatibilities [36]. Triton X-100 (Triton) is selected for this study. To minimize droplet agglomeration, the Triton is added to the RSF solution. In this set of experiments, the dialysis time for the RSF solution is 24 hr and the focus ratio is set to 1, where sheath and ink rate are 20 sccm or (20,20). More specifically, one drop of Triton (~0.05ml) from pipette was added to 0.5 ml silk fibroin solution in the vial and mixed well, thus the RSF solution is of 10% Triton. This is a relatively very high concentration compared to what Li et al. used, which was 5 to 80 mmol/L of final surfactant concentration in silk fibroin concentration of 10 to 15 wt% [36]. The ink and sheath rates are relatively low for sufficient liquid droplets to be deposited onto the substrate. After depositing with Triton, as shown in Figure 12 (b), it is observed that the material is deposited more densely though overspray still exists along the edge; however, the morphology of the individual particles are visually the same, for the pattern with or without Triton. The material is found to become denser with only an 8% line width increase after adding Triton with the aid of ImageJ. The material composition

and pattern geometry are further analyzed to ensure that the dense material is not purely Triton and if there exist other effects on the feature size.

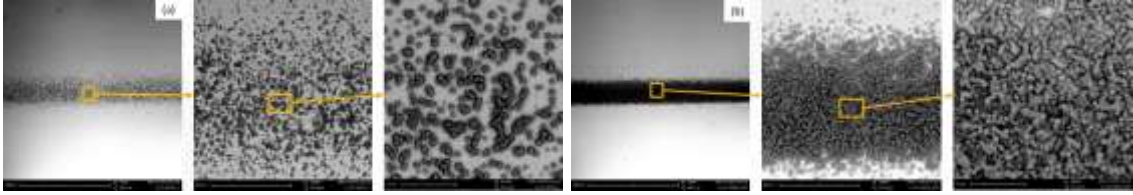


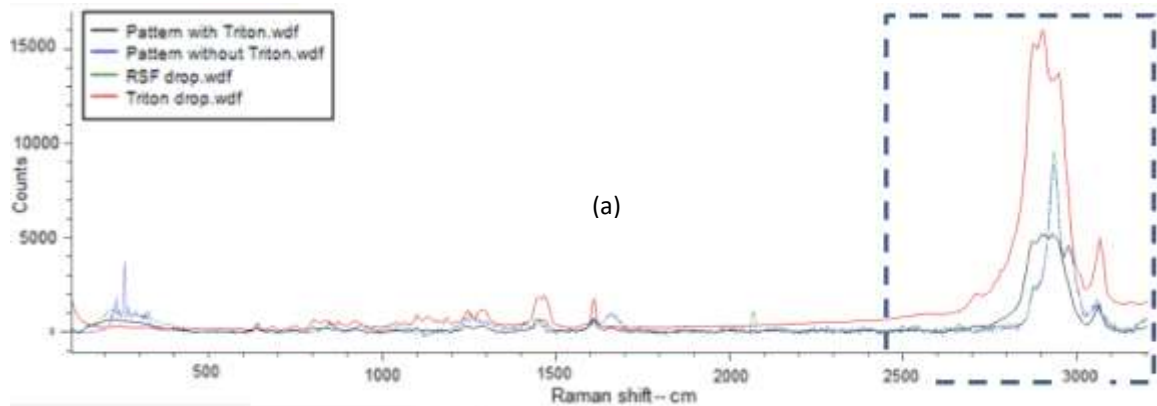
Figure 12. Pattern deposition (a) before and (b) after adding Triton

3.4.1 Impact of Triton on Pattern Composition

Raman spectra for four different materials (plain Triton, RSF solution, and the patterns with and without Triton) are overlapped in Figure 13. To get the materials on the same scale baseline subtraction with same settings, including laser type, laser power, exposure time, and scanning range, had to be performed. Several datasets are gathered for each material group, red being the liquid state of Triton, green being the liquid state of RSF, blue being the printed pattern without Triton, and black being the printed pattern with Triton. The best representative curve with less noise and reasonable amounts of intensities are picked for the comparison. As suggested previously, the effective way for analyzing this material is at the highest intensity of the spectra, around 2,900 - 3,000 shift-cm.

From the boxed area in Figure 13 (b) where three curves are normalized to the same scale, it can be seen that the curves of the RSF drop and Triton drop both contribute to the shape of the pattern with Triton. This suggests that the printed pattern contains both

Triton and silk fibroin, as would be expected. Quantitatively, the datasets of the two curves are scaled down by A and B from Figure 13 (b) to (c) to force the sum of peak values of the RSF drop (green) and the Triton drop (red) to be equal to the pattern with Triton (black). The ratio of A to B determines the ratio of Triton to silk fibroin in the final pattern, which is found to be 3.9 to 1.1, hence the ratio of Triton to RSF in the final pattern is 3.55, which remains relatively close to the original ratio of 3.7 in liquid state before printing. However, this is only an approximate approach for quantitatively analyzing the composition in printed pattern using Raman since there exists a large variation in intensities between different samples. Although Triton was shown to help with material dispersion and pattern uniformity, more research is needed to determine if it is truly an effective surfactant for aiding with aerosol jet printing RSF solution.



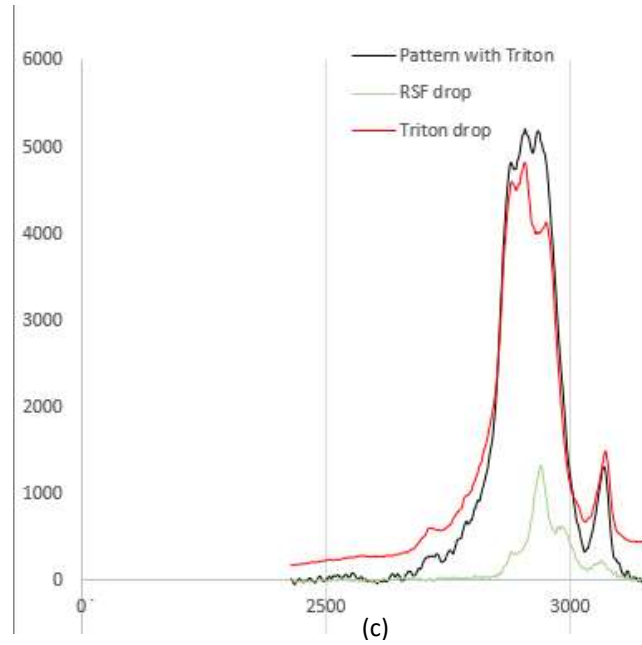
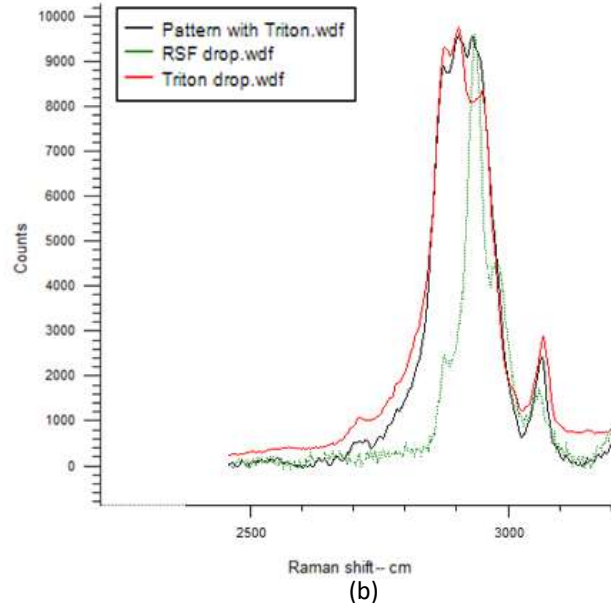


Figure 13. (a)Full range Raman spectra (b) Selected region for Raman analysis (c) After linear combination

3.4.2 Impact of Triton on Pattern Geometry

When the AJP processing parameters are set closer to the operating window boundary limits, Triton has minimal impact on the pattern feature size. For example, the

focus ratio (FR) is 1 for a range of processing conditions, e.g., (20, 20) or (25, 25); however, its impact on feature size will be different. At (20, 20) the feature size only increased by 8%, whereas for (25, 25) the feature size increased by 80%. This is possibly because, in the latter case, when $FR=1$ the ink rate increases by 5 sccm, providing an opportunity to produce many more fine liquid droplets compared with the solid particles produces when the ink rate is below 25. When the focus ratio is increased to more than 2, by increasing only the sheath rate, the feature size increases by less than 20%. This suggests that Triton is more applicable when being added to patterns that are processed at the lower margin of the operating window, meaning the leftmost boundary limit, since fine solid particles would be deposited. RSF solutions with and without Triton under different processing conditions are used to produce patterns. Therefore, the line width increases by 49% on average when the ink rate is kept in a range of 20 to 25 and the FR is in a range from 1 to 5. Beyond investigating the feature size trend on line pattern, the change in thickness change is also studied based on circular patterns, since larger area enables a better understanding of the whole geometry and challenges that may be faced in the real applications.

The general trend of the impact on thickness is that the Triton increases the thickness by 5 times of its original thickness. It should be noted that many of the patterns, ultimately due to the substrate exhibiting concavity, making the thickness measurement tougher using the typical optical profiler or contact profilometry. In this work, a Keyence VK-X laser scanning microscope, which enables an auto-fix of the concavity at the baseline, is used for a more accurate thickness data. For thickness measurement, two scans across circle CenterPoint are needed for each pattern, one vertically and one

horizontally. A comparison between the pattern without and with Triton added is shown in Figures 14 (a and b). The height magnification is enlarged to 160 times of its real size to show the exaggerated view to better observe the morphology. It can be seen that the amount of small particles or droplets does not change by adding Triton. Furthermore, as shown in Figures 14 (c and d) from the SEM images, the overspray around the circle still existed for both patterns, which suggests that Triton would be effective in helping to disperse the material, though, making the deposited pattern thicker with a slightly larger feature size, but not effective for reducing overspray. Comparing the percentage of composition to the thickness change after adding Triton suggests that the original thickness is enhanced by 2.4 times due to the influence of Triton, because of the focused aerosol stream at lower margin of operating window, along with possible reduced ink evaporation rate so that more material is eventually deposited [10].

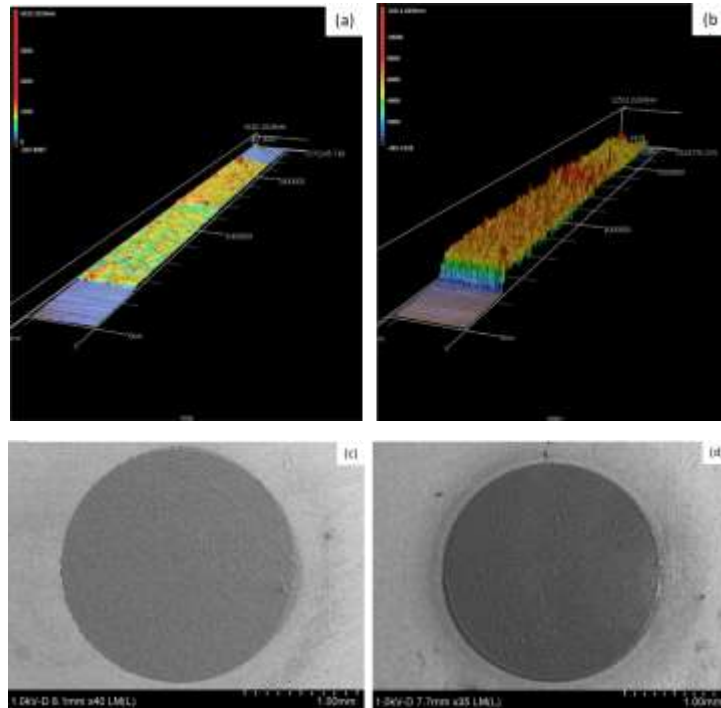


Figure 14. 3D image of pattern without(a) and with(b) Triton

Line widths as a function of FR for different ink rates with and without Triton are shown in Figure 15. When Triton is added to the RSF solution, the line width doubles in size compared to the line width formed without Triton at low FR. There exists a local minimum at around FR of 3 before a significant raise when Triton is added to the RSF solution. When Triton is added, as the ink rate increases the feature size drastically increases as the FR 3 or 4, suggesting that a large amount of liquid droplets form creating a pooling effect. Ink rate of 23 sccm has the smallest line width 10 μm , which is on the order of the resolution of the AJP.

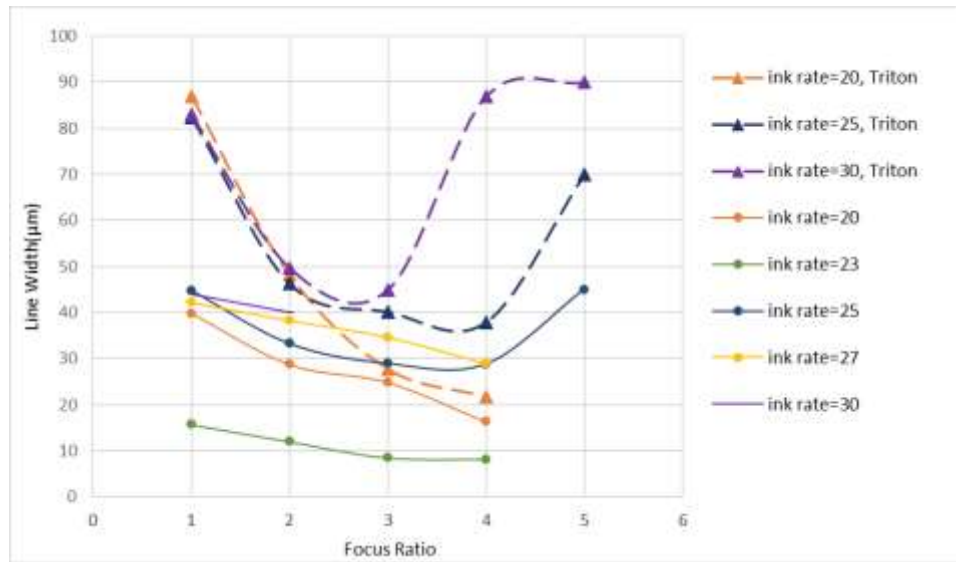


Figure 15. Relationship between line width and focus ration as a function of ink rate for RSF solution with and without Triton

3.5 Effect of Focus Ratio on Printed Pattern

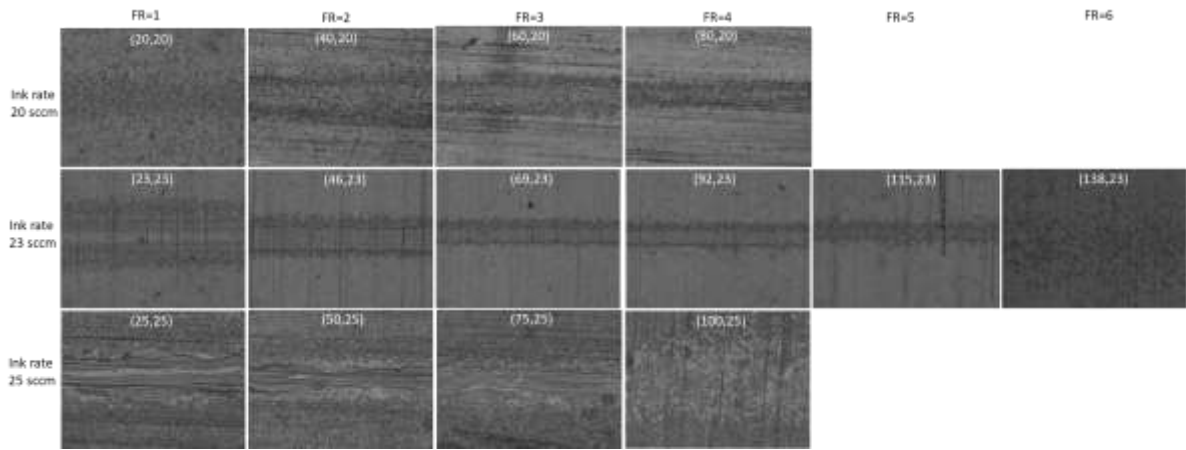
Several studies have found that increased FR decreases feature size and reduces overspray. Each has shown local minimum when printing line patterns of silver

nanoparticles. Continuing to increase FR when it exceeds a certain limit leads to less qualified pattern [27, 29, 31]. In this section, the impact of FR on printed pattern is further studied regarding to its benefit for improving pattern quality in the aspects of pattern feature size and amount of overspray.

3.5.1 Impact of Focus Ratio on Pattern Geometry

A representative group of optical images of lines and circles for better understanding of overspray and pooling phenomena are shown in Figure 14. Different ink rates with a 3 sccm step size are shown in each row, while FRs from 1 to 6 are shown in the columns. It is evident from this group of images that several trends exist. Ink rates of 20 sccm and 25 sccm are at the margin of the operating window, fine solid particles are difficult to produce when ink rate is lower than 20 sccm, leading to non-focusing of the AJP and ink rate larger than 25 sccm produces too many fine liquid droplets leading to pooling and a deformed pattern. From the entire set of images, it is found that the non-focusing phenomenon occurs either when the ink rate is around 20 with a low FR or at the optimum range with a high FR. Pooling occurs mainly at the upper margin of the ink rate range and deteriorates with an increasing FR. There appears to be hard for FR to rise up to 6 when ink rate is at boundary limits. Nevertheless, if there is system drift, it may be possible to process the RSF solution at $FR = 6$ at 20 sccm ink rate, however at an ink rate of 25 sccm FR may decrease to 2 as implied in Figure 9, because system drift, as its name implies, would lead to shift of operating window instead of altering the operating window.

It has been demonstrated that the line pattern gets more focused and thinner as the FR decreases, and then reaches a local minimum depending upon on the FR and ink rate, e.g., FR = 4 and ink rate 20 sccm, FR = 5 and ink rate 23 sccm, and FR = 2.5 and ink rate 25 sccm. This trend implies that the overspray first reduces with increasing FR but will then get worse as FR increases. System drift can easily change the location of the local minimum though. Similarly for circle patterns printed with an ink rate of 23 sccm, the



diameter of the circle decreases as the sheath rate increases, as shown in Figure 17. A local minimum exists at a FR of 4. It is evident from these figures that the size of the overspray ring is approximately the same, whereas the intensity of the overspray reduces as the sheath rate increases. These trends agree with those observed by Chen et al and Smith et al, when printing Norland Electronic Adhesives (NEA) aerosolized ink and silver nanoparticles [27, 31]. Similarly, the phenomena here of printing RSF can be understood as increased sheath rate is beneficial for creating focused beam being deposited onto substrate, which makes the line pattern thinner. However, this cannot be indefinitely optimized due to the fact that very high sheath rate within the nozzle can alter the flow property from laminar to turbulent flow, which eventually causes the broadening of printed pattern for both line pattern and overspray [27].

Figure 16. Optical images for the influence of process parameters on line morphology

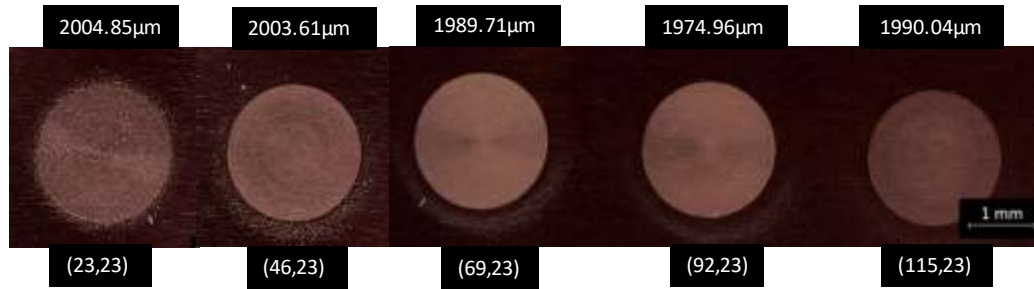


Figure 17. Circle pattern with increasing FR at ink rate of 23 sccm

3.5.1.1 Impact of Focus Ratio on Line Width

The directional relationship between FR and line width under various conditions, such as material, dialysis time, processing parameters, is shown in Figure 18. The line widths of the patterns are measured using ImageJ, across at least six data points to get the average line width (e.g., feature size). The line width decreases as FR increases, with or without Triton or for a dialysis time of 24 hr or 48 hr, as shown in Figures 18 (a and b). Similar trends have been shown for varying AJP process parameters and ink formulations [27, 29]. Figure 18 (a) aims to demonstrate the same trend it has shown even with system drift existing at two different batch produced at 6 months apart with different dialysis time. Variation occurs when FR is above 3, which mainly results from system drift of the AJP when operating with different environmental factors, e.g., humidity and temperature during the material fabrication. The line widths range from 75 μm to 85 μm initially, then gradually decreases to as low as 20 μm, depending on the ink rate. For an ink rate of 25

sccm and dialysis time of 48 hr, the FR has a local FR = 3.5 and peaks at 5. A similar trend has been observed by Chen et al. recently when printing NEA aerosolized ink, with the finding that the overspray decreases then increases as the sheath rate increases up to 300 sccm [31], meanwhile the local minimum of RSF prints shows up at a much lower sheath rate. This is likely caused by the viscosity difference of these two materials, which can be explained by the Reynolds Number shown below, where V is the velocity, ρ is density, d is diameter, μ and ν are the dynamic and kinematic viscosities, respectively. NEA 121 ink has a viscosity of 300 cP, which is more than 100 times of viscosity of RSF solution. Thus, based on the Reynolds number, it is evident that the velocity has a larger impact on lower viscosity, which explains the reason why aerosol jet printing RSF solution has a smaller local minimum compared with other metallic inks.

$$Re = \frac{\rho V d}{\mu} = \frac{V d}{\nu}$$

When variations from environmental factors are eliminated, the data is more consistent as illustrated in Figure 18 (b). The line width decreases as the FR increases even when FR is less than 1. To this end, the experiments have to be performed at FR from 1 to 6, since this range allows for a minimized line width. Although the line width increases, when one drop of Triton is added, the same trend is observed. It is also evident that the slope of line width decrement is faster as the FR is smaller than 1. For instance, when the sheath rate is held still at 20 sccm, increasing ink rate from 20 sccm to 50 sccm generates a 51% decrease of line width from 68 μm to 45 μm . This may suggest that when the sheath rate is held still, ink rate performs a larger influence on the printed pattern comparing with having ink rate remained the same. As a result, such findings can

be applied to the scenarios that have constraints of increasing sheath rate. Line width can be reduced by setting $FR < 1$ for a given sheath rate.

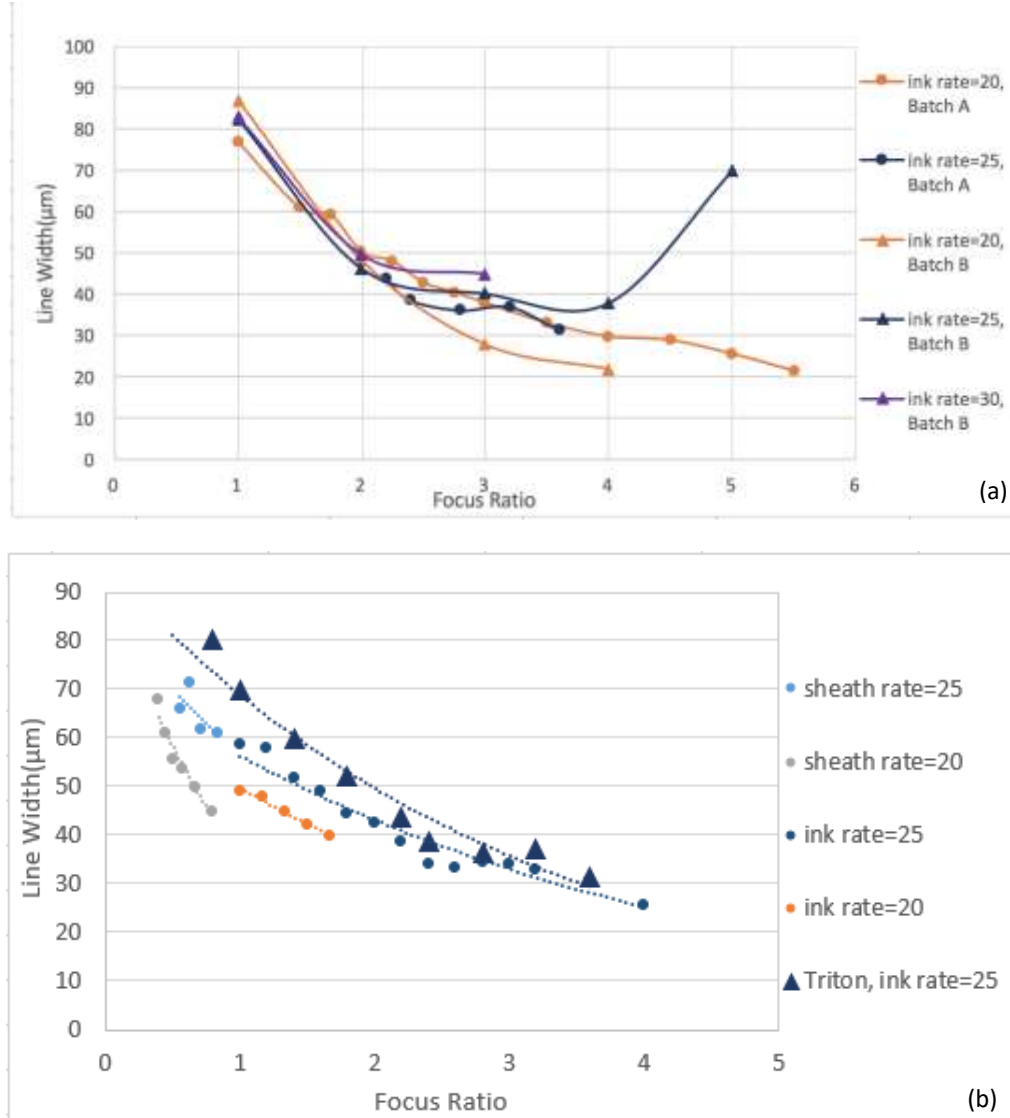


Figure 18. Influence of focus ratio (FR) on line width (a) all with Triton and (b) all on same run

3.5.1.2 Impact of Focus Ratio on Line Thickness

The relationship between FR and pattern thickness, i.e., z-height, is shown in Figure 19. The curve converges as FR reaches 4. This is because larger FR either induces

non-focusing or there are too few fine solid particles to measure. With the exception of an ink rate of 30, which exhibited pooling, the thickness decreases with increasing FR, which is contrary to what has been observed when AJ printing lines of silver nanoparticles [27]. It is believed that at larger FR the printed patterns generates a non-focusing state at a range of 100 nm to 150 nm thickness. Furthermore, it is believed that compressibility of RSF solution makes it perform differently with metallic inks, which explains the decreased thickness with increased FR. Additionally, it could be due to a higher sensitivity of ink evaporation under increased sheath rate.

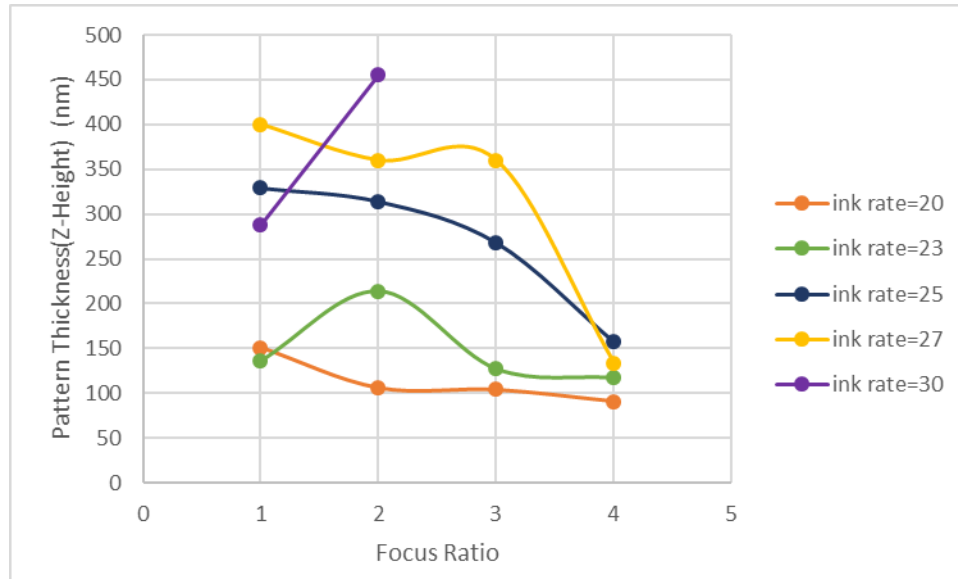
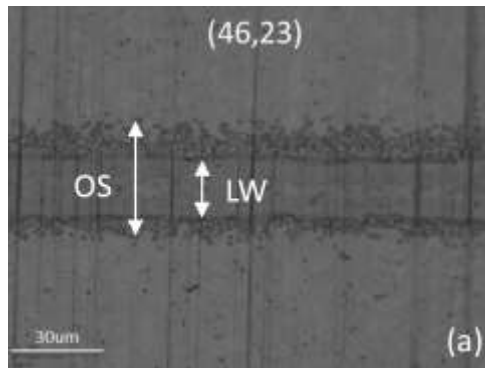


Figure 19. Influence of focus ratio (FR) on pattern thickness

3.5.2 Impact of Focus Ratio on Overspray

As previously stated, Triton is not effective for reducing overspray. The relationship between FR and overspray is shown in Figure 20, for 48 hr dialysis with 2.7%

concentration RSF solution based on measured line width (LW) and the line pattern with overspray (OS). As an example, image (46, 23) illustrates a line path with some aerosols scattered along the edge of the line pattern, which is OS, and a clearly defined line width, LW. To produce Figure 20 (b), LW is measured and the overspray size is obtained by deducting the line width from the measured OS. It can be seen that the overspray is the lowest (10 μm) when FR is highest (4), when the ink rate is relatively low, at 20 sccm and 23 sccm. However, as ink rate increases, 25 sccm and 27 sccm, a local minimum at around 3 to 4 exists, just before a significant increase in line width, which suggests the occurrence of less focusing. Overspray is initially 40 μm , with the exception of an ink rate of 27 due to pooling, and decreases as FR increases or line width decreases. Hence, FR and line width are correlated and influence overspray phenomena, though it seems that it is more sensitive to line width. An important observation from this data is that an ink rate of 23 generates the finest feature size no matter what FR is, which means the overspray phenomena can be most effectively reduced at an ink rate of 23.



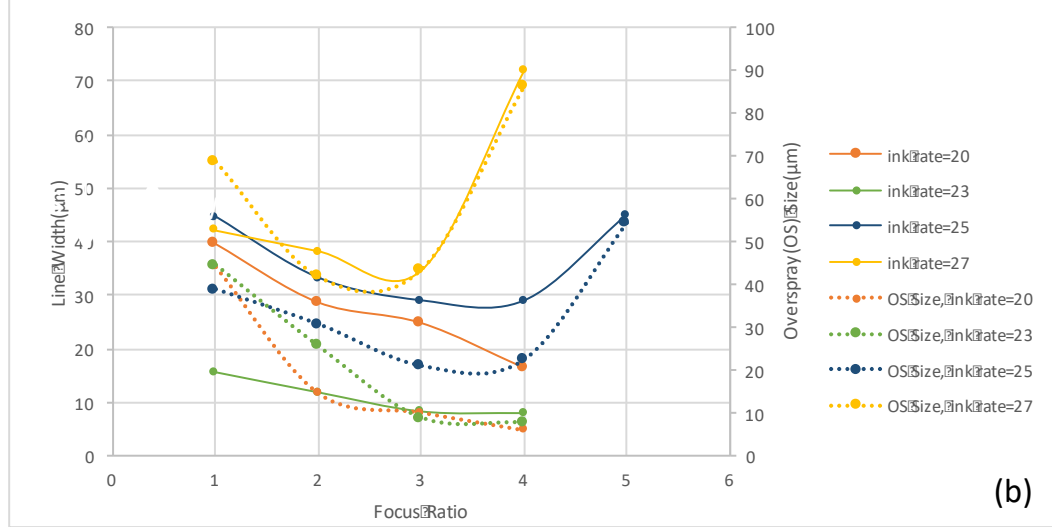


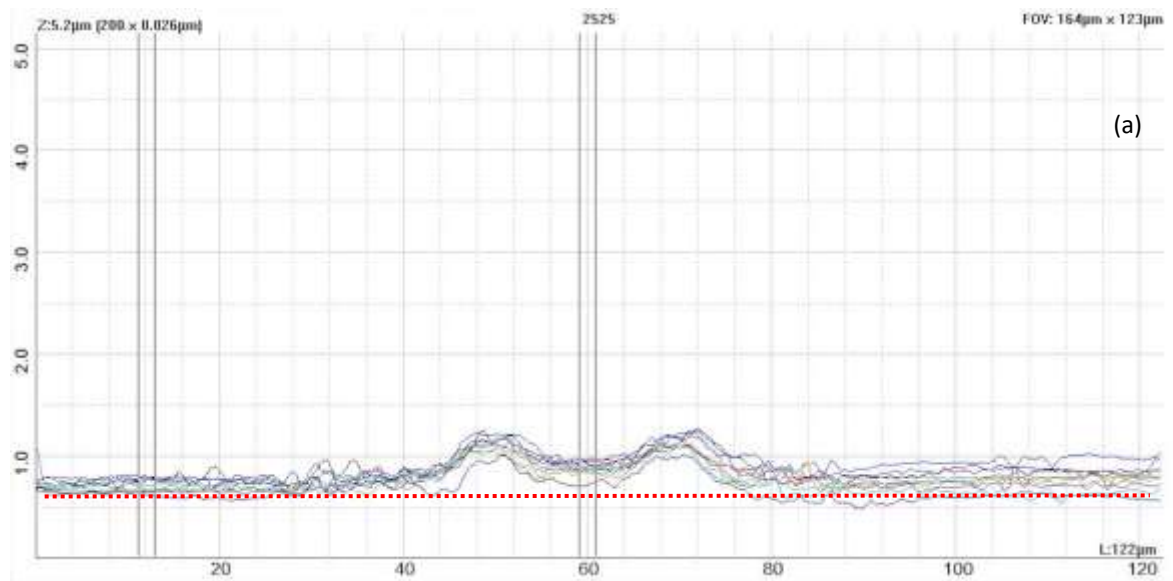
Figure 20. (a) Overspray definition. (b) Influence of focus ratio (FR) on overspray

3.6 Challenges

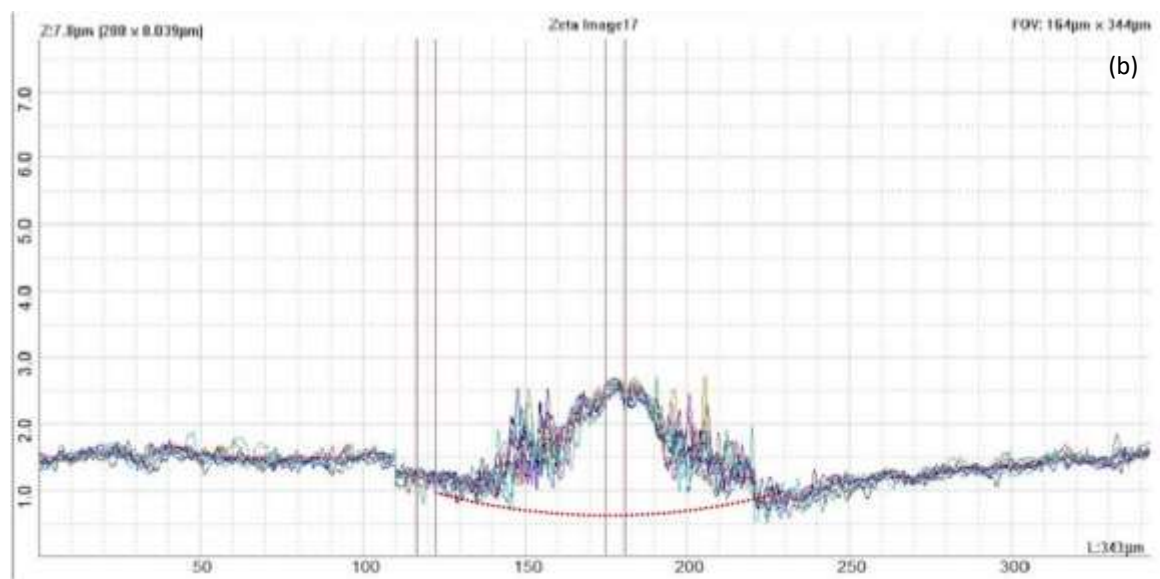
There exist some challenges in each step of this series of experiment, including material preparation, AJP fabrication, and post-processing of printed pattern. In material preparation involves unknown factors that can affect the protocol and make the produced RSF solution vulnerable to the AJP environment. Therefore, even though there is a study showing that dissolved silk solution can be reserved for up to 1 month [24], in this work, the material preparation protocol for making the RSF solution is repeated each time, unless otherwise noted. The sitting time in between each step during material preparation is minimized to ensure the freshness of the solution. Even so, the transport time between laboratory rooms, the time silk fibroin solution is exposed to surrounding air, and human error may make the final RSF solution deviate by different degrees from each other. It is

necessary to develop a more reliable technique to qualify or quantify the freshness and stability of the solution. The system drift during AJP processing is also something that requires more attention for calibrating the system, especially for biomaterials that are sensitive to the environmental factors. The other challenges induced from post processing of samples include the small amount of material contained in each sample. This limits the amount of analysis that can be conducted; for example the water content could not be measured using Thermogravimetric (TGA) analysis, which could help understand changes in geometric factors.

The thickness measurement results for line patterns using optical profiler are shown in the Figures 21 (a and b). A good substrate without substrate concavity is shown in Figure 21 (a) while the substrate with concavity is shown in Figure 21 (b). To better observe these results, red dashed lines are marked to help with the observation. The two convexities shown in Figure 21 (a) is the coffee ring effect during printing which makes the edge of the pattern higher than the center. This structure is difficult for measuring thickness across the surface, especially for small thickness values when there is no surfactant added, and it occurs for almost half of the patterns no matter circles or lines. As such, using alternative substrates such as silicon wafers could help manage the flatness of the samples.



(a)



(b)

Figure 21. (a) Cross-sectional view of RSF on copper substrate (b) Cross-sectional view of RSF on copper substrate showing the concavity

3.7 Summary

In short, besides providing modified protocol for formulating aerosol jet printable RSF solutions, Chapter 3 introduces the general trend that the quality of printed pattern can be optimized via varying sheath rate and ink rate, with the supports of qualitative and quantitative results of the influences of Triton and FR. Criteria table of qualifying AJP defects and operating window provides a clear pathway when attempting to minimize the line width for potential macroscale and microscale applications.

CHAPTER 4. CONCLUSION

This research work helped understand several advantages of fabricating silk fibroin via a novel scalable additive manufacturing technique, Aerosol Jet Printer, over other additive or conventional methods, with a main competitor of ink jet printer. Furthermore, it showcases the feasibility of printing silk fibroin solution using AJP, with the finding that regenerated silk fibroin solution with increased degumming and dissolution time and some other minor modifications becomes printable on AJP without any additives like reagents or other biocompounds, which overcomes the main limitation AJP has been having on processing silk fibroin. The procedure described in this work makes it suitable for ultrasonic atomizer, which will not lead to gelation compared with other's work before. Although the fidelity of printing process and system drift is still being studied, several important findings can be concluded here. First, agglomerations are hard to avoid, especially when such sensitive solution like RFS needs to undergo ultrasonic atomization. However, adding Triton X-100, a nonionic surfactant, was proved to be contributing for dispersion and eliminating large visible particles, which can be one top issue for handling RSF solution after atomization. Meanwhile, adding Triton may have altered the printed pattern with a significant increase in thickness and feature size, which needs to be taken into consideration since this can be pros or cons depending on different kinds of applications. Second, the top concerns of having overspray in AJP, can be minimized by identifying the optimum process parameters in multiple operating window which may include system drifts after several trial runs, but not necessarily with adding Triton. Additionally, a directional relationship was found between line width and

focus ratio for printing RSF solution that increasing focus ratio can decrease line width and overspray before the local minimum point, which will contribute to minimizing feature size and spatial resolutions, especially in micro level applications. Such trend applies to pattern with Triton added as well, with the only unfavorable influence that it might increase the feature size by 30% to 100% depending on the FR selected to print. More importantly, an optimum operating window with criteria were presented so that the researchers can reproduce or make improvements to the current protocol during their future in-depth studies on aerosol jet printing silk fibroin solution. Using ink rate of 20 sccm and 23 sccm to begin the tuning process to grasp a general idea of how such material performs in another environmental lab setting is necessary to apply corresponding adjustments for better outputs considering the system drift.

CHAPTER 5. FUTURE WORK

This thesis work only focuses on the influence of sheath and ink rate on the printed pattern. There are many other aspects people can keep investigating on, such as platen temperature, stage speed, working distance, etc., which will be contributing to understanding and tackling with overspray. The future study could select a better substrate for studying on the effect of FR to pattern thickness, which certainly needs to be understood by researchers. There are still many opportunities to develop for producing a more precise procedure with least variations caused from environmental factors from the perspective of the protocol. For instance, shortening material preparation time or reduce the necessities for the protocol to be repeated for AJP runs can make the whole process more productive. The surfactant effect can be further studied since it is found to be significantly help with dispersion from the final pattern morphology. More quantitative approach can be utilized, such as by tagging RSF solution and Triton with different uncommon elements for unique vibrational characteristics for easier quantification using Raman spectroscopy, to investigate the amount of Triton contained in the final pattern to better understand the role it plays. Otherwise, a better sample preparation should be done for using Raman spectrometer to study on the sample composition to get a relatively close intensities on different samples.

Most importantly, the stability of both RSF solution and AJP need to be further studied, more qualitative or quantitative methods other than visual inspection should be developed in the future to monitor the quality of ink and to keep track of AJP performance without spending large amount of time on tuning before conducting official

runs. Functionality testing can be considered as a reassurance step according to corresponding needs in different fields. More functionality or biological testing will be implemented if this topic is going to be expanded into specific application area; thus lowering the degumming time to below 1 hour may be worth being tested as well to increase its suitability for medical applications which requires high cell viability. More excitingly, a specific application area can be confirmed which would offer a clearer motivation and goal for such work once all parametric studies mentioned before are understood and aligned well with the current knowledge.

The protocol and AJP should be tuned for a general guide and need to be adapted to each individual lab setting by considering both environmental factors and physical AJP system. Some examples in Chapter 3 may exhibit different morphology even under same processing parameters on the same run, or with same processing parameters right after the solution is made on different days. A more detailed study on the system drift of aerosol jet printing silk fibroin may be conducted in the future.

REFERENCES

- [1] Altman, G.H., et al., *Silk-based biomaterials*. Biomaterials, 2003. **24**(3): p. 401-416.
- [2] Huang, Y., et al., *Silk fibroin films for potential applications in controlled release*. *Reactive and Functional Polymers*, 2017. 116(Supplement C): p. 57-68.
- [3] Mottaghitalab, F., et al., *Silk fibroin nanoparticle as a novel drug delivery system*. *J Control Release*, 2015. 206: p. 161-76.
- [4] Marelli, B., et al., *Silk Fibroin as Edible Coating for Perishable Food Preservation*. *Sci Rep*, 2016. 6: p. 25263.
- [5] Zhang, W., et al., *Silk Fibroin Biomaterial Shows Safe and Effective Wound Healing in Animal Models and a Randomized Controlled Clinical Trial*. *Advanced Healthcare Materials*, 2017. 6(10): p. 1700121.
- [6] Ghosh, S., et al., *Direct - Write Assembly of Microperiodic Silk Fibroin Scaffolds for Tissue Engineering Applications*. *Advanced Functional Materials*, 2008. **18**(13): p. 1883-1889.
- [7] Johnston, A.P.R., et al., *Layer-by-layer engineered capsules and their applications*. *Current Opinion in Colloid & Interface Science*, 2006. **11**(4): p. 203-209.
- [8] Parker Sara, T., et al., *Biocompatible Silk Printed Optical Waveguides*. *Advanced Materials*, 2009. **21**(23): p. 2411-2415.
- [9] K. Hon, L. Li, I. Hutchings *Direct writing technology—advances and developments*, *CIRP Ann-Manuf Technol*, 57 (2) (2008), pp. 601-620

- [10] H. Tao, B. Marelli, M. Yang, B. An, M.S. Onses, J.A. Rogers, D.L. Kaplan, F.G. Omenetto *Inkjet printing of regenerated silk fibroin: from printable forms to printable functions* Adv. Mater., 27 (29) (Aug. 2015), pp. 4273-4279
- [11] Dickerson, M. B.; Dennis, P. B.; Tondiglia, V. P.; Nadeau, L. J.; Singh, K. M.; Drummy, L. F.; Partlow, B. P.; Brown, D. P.; Omenetto, F. G.; Kaplan, D. L. *3D Printing of Regenerated Silk Fibroin and Antibody-Containing Microstructures via Multiphoton Lithography*. ACS Biomater. Sci. Eng. 2017, 3 (9), 2064–2075.
- [12] Vaseem, M., et al., *Inkjet Printed Fractal-Connected Electrodes with Silver Nanoparticle Ink*. ACS Applied Materials & Interfaces, 2012. 4(6): p. 3300-3307.
- [13] K. K. B. Hon, L. Li, and I. M. Hutchings, *Direct writing technology—advances and developments*, CIRP Annals, vol. 57, no. 2, pp. 601–620, 2008.
- [14] Zhang, Y.; Liu, C.; Whalley, D. *Direct-Write Techniques for Maskless Production of Microelectronics: A Review of Current State-of-the-Art Technologies*. In International Conference on Electronic Packaging Technology & High Density Packaging (ICEPT-HDP); Beijing, China, 2009; p 497
- [15] Cummins, G., & Desmulliez, M. P. Y. (2012). *Inkjet printing of conductive materials: a review*. Circuit World, 38(4), 193-213.
- [16] S.H. Hashimdeen, M. Miodownik, M.J. Edirisinghe. *Print head design and control for electrohydrodynamic printing of silk fibroin* Mater. Sci. Eng. C, 33 (2013), pp. 3309-3318
- [17] Chawla, S.; Midha, S.; Sharma, A.; Ghosh, S. *Silk-based bioinks for 3D bioprinting*. Adv. Healthc. Mater. **2018**, 7, 1701204.
- [18] Hoath S, Martin G D and Hutchings I M 2010 *Effects of fluid viscosity on drop-on-demand ink-jet break-off* NIP26 Digit. Fabr. 2010 pp 10–3
- [19] Delaney J T, Smith P J and Schubert U S, *Inkjet printing of proteins* Soft Matter, 2009, **5** 4866–77

- [20] S. Khalil, J. Nam, W. Sun *Multi-nozzle deposition for construction of 3D biopolymer tissue scaffolds Rapid Prototyping J*, 11 (2005), pp. 9-17
- [21] H. Wang, Y. Zhang, H. Shao, X. Hu *A study on the flow stability of regenerated silk fibroin aqueous solution Int J Biol Macromol*, 36 (2005), pp. 66-70
- [22] T. Billiet, M. Vandenhaute, J. Schelfhout, S. Van Vlierberghe, P. Dubrue, *A review of trends and limitations in hydrogel-rapid prototyping for tissue engineering*, Biomaterials, 33 (2012), pp. 6020-6041 [23] Sen A K and Darabi J. *Droplet ejection performance of a monolithic thermal inkjet print head J. Micromech. Microeng.* 2007. **17** 1420-7
- [24] Rockwood, D.N., et al., *Materials fabrication from Bombyx mori silk fibroin*. Nat Protoc, 2011. 6(10): p. 1612-31.
- [25] M. Mondal, K. Trivedy, S. Nirmal Kumar Caspian J. Environ. Sci., 5 *The silk proteins , sericin and fibroin in silkworm , Bombyx mori.* (2007), pp. 63-76
- [26] Vollrath, F. and D. Porter, *Silks as ancient models for modern polymers*. Polymer, 2009. 50(24): p. 5623-5632.
- [27] Michael, S., et al., *Controlling and assessing the quality of aerosol jet printed features for large area and flexible electronics. Flexible and Printed Electronics*, 2017. 2(1): p. 015004.
- [28] Benjamin, JA, Rajkhowa, R, Dilley, RJ *The impact of degumming conditions on the properties of silk films for biomedical applications*. Text Res J 2016; 86: 275–287.
- [29] Mahajan, A., C.D. Frisbie, and L.F. Francis, *Optimization of Aerosol Jet Printing for High-Resolution, High-Aspect Ratio Silver Lines*. ACS Applied Materials & Interfaces, 2013.5(11): p. 4856-4864.
- [30] Vaseem, M., et al., *Inkjet Printed Fractal-Connected Electrodes with Silver Nanoparticle Ink*. ACS Applied Materials & Interfaces, 2012. 4(6): p. 3300-3307.

- [31] Chen, G., Gu, Y., Tsang, H., Hines, D. R., and Das, S., 2018, *The Effect of Droplet Sizes on Overspray in Aerosol - Jet Printing*, Advanced Engineering Materials, 2018, pp. 1701084- 1701084.
- [32] Goth, C., S. Putzo, and J. Franke, *Aerosol Jet printing on rapid prototyping materials for fine pitch electronic applications*. 2011. p. 1211-1216.
- [33] Direct-Write Technologies for Rapid Prototyping Applications: Sensors, Electronics, and Integrated Power Sources; Piqué, A., Chrisey, D. B., Eds.; Academic Press: San Diego, CA, 2002.
- [33] Justin M. Hoey, Artur Lutfurakhmanov, Douglas L. Schulz, and Iskander S. Akhatov, *A Review on Aerosol-Based Direct-Write and Its Applications for Microelectronics*, Journal of Nanotechnology, vol. 2012, Article ID 324380, 22 pages, 2012.
- [34] Rider, P.; Zhang, Y.; Tse, C.C.W.; Zhang, Y.; Jayawardane, D.; Stringer, J.; Callaghan, J.; Brook, I.M.; Miller, C.A.; Zhao, X.; et al. *Biocompatible silk fibroin scaffold prepared by reactive inkjet printing*. J. Mater. Sci. **2016**, 51, 8625–8630.
- [35] S.D. Risio, N. Yan, *Piezoelectric ink-jet printing of horseradish peroxidase: effect of ink viscosity modifiers on activity* Macromol. Rapid Commun., 28 (2007), pp. 1934-1940
- [36]_Zhao Li, Zhaokun Zheng, Yuhong Yang, Guangqiang Fang, Jinrong Yao, Zhengzhong Shao, and Xin Chen, *Robust Protein Hydrogels from Silkworm Silk*, ACS Sustainable Chemistry & Engineering **2016** 4 (3), 1500-1506
- [37] D. Ngo and S. Baldelli, *J. Phys. Chem. B*, 2016, **120**, 12346 – 12357